



THE UNIVERSITY *of* EDINBURGH

Edinburgh Research Explorer

Last millennium Northern Hemisphere summer temperatures from tree rings: Part II, spatially resolved reconstructions.

Citation for published version:

Anchukaitis, K, Wilson, R, Briffa, KR, Cook, ER, D'Arrigo, R, Davi, N, Esper, J, Frank, D, Gunnarson, BE, Hegerl, G, Helama, S, Klesse, S, Krusic, P, Linderholm, HW, Myglan, V, Osborn, TJ, Zhang, P, Rydval, M, Schneider, L, Schurer, A, Wiles, G & Zorita, E 2017, 'Last millennium Northern Hemisphere summer temperatures from tree rings: Part II, spatially resolved reconstructions.', *Quaternary Science Reviews*.
<https://doi.org/10.1016/j.quascirev.2017.02.020>

Digital Object Identifier (DOI):

[10.1016/j.quascirev.2017.02.020](https://doi.org/10.1016/j.quascirev.2017.02.020)

Link:

[Link to publication record in Edinburgh Research Explorer](#)

Document Version:

Peer reviewed version

Published In:

Quaternary Science Reviews

General rights

Copyright for the publications made accessible via the Edinburgh Research Explorer is retained by the author(s) and / or other copyright owners and it is a condition of accessing these publications that users recognise and abide by the legal requirements associated with these rights.

Take down policy

The University of Edinburgh has made every reasonable effort to ensure that Edinburgh Research Explorer content complies with UK legislation. If you believe that the public display of this file breaches copyright please contact openaccess@ed.ac.uk providing details, and we will remove access to the work immediately and investigate your claim.



Last millennium Northern Hemisphere summer temperatures from tree rings: Part II, spatially resolved reconstructions

Kevin J. Anchukaitis^{a,b,c,*}, Rob Wilson^{d,e}, Keith R. Briffa^e, Ulf Büntgen^{f,g,h}, Edward R. Cook^c, Rosanne D'Arrigo^c, Nicole Davi^{c,i}, Jan Esper^j, David Frank^{b,g}, Björn E. Gunnarson^k, Gabi Hegerl^l, Samuli Helama^m, Stefan Klesse^{b,g}, Paul J. Krusic^{k,c,n}, Hans W. Linderholm^o, Vladimir Myglan^p, Timothy J. Osborn^e, Peng Zhang^o, Milos Rydval^{d,q}, Lea Schneider^r, Andrew Schurer^l, Greg Wiles^s, Eduardo Zorita^t

^a*School of Geography and Development, University of Arizona, Tucson, AZ, USA*

^b*Laboratory of Tree-Ring Research, University of Arizona, Tucson, AZ, USA*

^c*Lamont-Doherty Earth Observatory of Columbia University, Palisades, NY, USA*

^d*School of Geography and Geosciences, University of St Andrews, UK*

^e*Climatic Research Unit, School of Environmental Sciences, University of East Anglia, Norwich, UK*

^f*Department of Geography, University of Cambridge, Cambridge, UK*

^g*Swiss Federal Research Institute WSL, Birmensdorf, Switzerland*

^h*Global Change Research Centre and Masaryk University Brno, Czech Republic*

ⁱ*Department of Environmental Science, William Paterson University, Wayne, NJ, USA*

^j*Department of Geography, Gutenberg University, Mainz, Germany*

^k*Department of Physical Geography, Stockholm University, Stockholm, Sweden*

^l*School of GeoSciences, University of Edinburgh, Edinburgh, UK*

^m*Natural Resources Institute Finland, Rovaniemi, Finland*

ⁿ*Navarino Environmental Obs., Messinia, Greece*

^o*Department of Earth Sciences, University of Gothenburg, Göteborg, Sweden*

^p*Siberian Federal University, Krasnoyarsk, Russia*

^q*Faculty of Forestry and Wood Sciences, Czech University of Life Sciences Prague, Czech Republic*

^r*Department of Geography, Justus Liebig University, Giessen, Germany*

^s*Tree Ring Lab, The College of Wooster, Wooster, OH, USA*

^t*Institute of Coastal Research, Helmholtz-Zentrum Geesthacht (HZG), Hamburg, Germany*

Abstract

Climate field reconstructions from networks of tree-ring proxy data can be used to characterize regional-scale climate changes, reveal spatial anomaly patterns associated with atmospheric circulation changes, radiative forcing, and large-scale modes of ocean-atmosphere variability, and provide spatiotemporal targets for climate model comparison and evaluation. Here we use a multiproxy

*Corresponding author

Email address: kanchukaitis@email.arizona.edu (Kevin J. Anchukaitis)

network of tree-ring chronologies to reconstruct spatially resolved warm season (May-August) mean temperatures across the extratropical Northern Hemisphere (40-90°N) using Point-by-Point Regression (PPR). The resulting annual maps of temperature anomalies (750 to 1988 CE) reveal a consistent imprint of volcanism, with 96% of reconstructed grid points experiencing colder conditions following eruptions. Solar influences are detected at the bicentennial (de Vries) frequency, although at other time scales the influence of insolation variability is weak. Approximately 90% of reconstructed grid points show warmer temperatures during the Medieval Climate Anomaly when compared to the Little Ice Age, although the magnitude varies spatially across the hemisphere. Estimates of field reconstruction skill through time and over space can guide future temporal extension and spatial expansion of the proxy network.

Keywords: Tree-rings, Northern hemisphere, Last millennium, Common Era, Summer temperatures, Reconstruction, spatial

1. Introduction

Global and hemispheric temperature anomalies reflect the influence of both internal variability in the climate system as well as the consequences of changes in radiative forcing, such as insolation, volcanic eruptions, and greenhouse gas concentrations. Surface temperature is determined by the planetary energy balance and serves as a symptom of perturbations to that balance, but also contains variability due to natural climate system dynamics. Rising global mean surface temperature is a key diagnostic for the influence of increasing greenhouse gases on the Earth's climate system. Yet changes in incoming solar radiation, orbital (Milankovich) changes, albedo and land use alterations, and natural and anthropogenic aerosols also influence surface temperatures. Different radiative forcing mechanisms as well as internal modes of coupled ocean-atmosphere variability may have distinct fingerprints on temperature anomalies across different spatial, temporal, and seasonal scales (Hegerl et al., 1997; Rind et al., 1999; Shindell et al., 2001b; Hegerl et al., 2003; Rind et al., 2004; Shindell et al., 2003, 2004;

16 Hegerl et al., 2006, 2007; Shindell and Faluvegi, 2009; Shindell, 2014; Shindell
17 et al., 2015). Surface temperature anomalies are therefore controlled by the
18 superposition of various external radiative and internal dynamical influences on
19 the climate system. Detection and attribution of the causes of temperature fluc-
20 tuations, as well as the prediction of future regional-scale changes, thus depend
21 on accurate quantification and understanding of spatial and temporal variations
22 in surface temperature (Hegerl et al., 1997; Stott and Tett, 1998; Meehl et al.,
23 2004; Lean and Rind, 2008; Stott and Jones, 2009; Stott et al., 2010; Solomon
24 et al., 2011; Hegerl and Stott, 2014).

25 Paleoclimate reconstructions of past temperature extend knowledge of cli-
26 mate system variability beyond that available from the limited instrumental
27 observational record. They offer longer timescales over which to observe a more
28 complete range of variability in solar and volcanic forcing, extended opportuni-
29 ties to characterize internal climate system fluctuations at decadal and longer
30 timescales, and the potential to separate forced and unforced responses to better
31 understand their magnitude and spatiotemporal patterns (Hegerl et al., 2003,
32 2007). Spatially-explicit reconstructions provide additional opportunities to re-
33 fine our understanding of fundamental climate system characteristics, diagnose
34 the influence of different forcings on various aspects of the climate system, and
35 provide insight into both regional climate changes and the response of large-
36 scale modes of ocean-atmosphere variability (Seager et al., 2007; Cook et al.,
37 2010a,b; Hegerl and Russon, 2011; Phipps et al., 2013; PAGES 2k-PMIP3 group,
38 2015; Goosse, 2016). Comparisons between palaeoclimatic data and models also
39 provide out-of-sample tests of the general circulation models (GCMs) used for
40 future climate projections and can indicate where the modeled forced response or
41 internal variability requires further evaluation and continued refinement. Such
42 comparisons may help constrain the probable range of model parameters or
43 identify the forcing configurations most consistent with past climate variabil-
44 ity (Edwards et al., 2007; Anchukaitis et al., 2010; Schmidt, 2010; Hegerl and
45 Russon, 2011; Brohan et al., 2012; Schurer et al., 2013; Schmidt et al., 2014;
46 Harrison et al., 2015; Tingley et al., 2015).

Reconstructions of last millennium and Common Era surface temperatures have focused predominantly on single time-series to represent continental- to global-scale variations in mean annual or growing season temperatures aggregated over space (Frank et al., 2010; Masson-Delmotte et al., 2013; PAGES2k, 2013; Stoffel et al., 2015; Smerdon and Pollack, 2016) while fewer have used climate field reconstruction (CFR) methods (Fritts, 1991; Cook et al., 1994; Evans et al., 2001; Tingley et al., 2012) to quantify past temperature anomalies simultaneously through time and across space (c.f. Mann et al., 1998; Tingley and Huybers, 2013; Wang et al., 2015). Spatial field reconstructions offer the benefit of characterizing regional-scale climate changes, can reveal spatial anomaly patterns or fingerprints associated with atmospheric circulation, radiative forcing, and large-scale modes of ocean-atmosphere variability, and provide complete spatiotemporal targets for GCM evaluation (Evans et al., 2001; Anchukaitis and McKay, 2014; Kaufman, 2014; Schmidt et al., 2014).

Here, we develop and evaluate a climate field reconstruction of extratropical Northern Hemisphere summer temperatures using an updated network of temperature-sensitive tree-ring proxy chronologies and existing temperature reconstructions back to 750 CE (Wilson et al., 2016). We are motivated by two fundamental challenges to the development of skillful large-scale last millennium temperature reconstructions revealed over the last two decades (c.f. Frank et al., 2010; Smerdon and Pollack, 2016): First, biases arising from characteristics of the proxies themselves; Second, uncertainties arising from the choice of reconstruction methodologies.

Tree-ring proxies provide precise annual dating and are broadly distributed across extra-tropical land areas, making them one of the most widely used proxies for climate reconstructions of the Common Era (Hughes, 2002; Jones et al., 2009; Smerdon and Pollack, 2016). Yet despite these advantages, certain challenges or limitations exist: they preferentially reflect growing season temperature conditions, they require some manner of processing to remove non-climatic age or tree geometry related growth trends, and there exist a wide range of climate responses amongst the more than two thousand tree-ring chronologies

78 currently archived in public repositories (Briffa, 1995, 2000; Briffa et al., 2002,
 79 2004; St. George, 2014; St George and Ault, 2014). A decade ago, D’Arrigo et al.
 80 (2006) and Wilson et al. (2007) used small high-latitude networks of tree-ring
 81 proxy chronologies to reconstruct mean annual Northern Hemisphere tempera-
 82 tures. These and subsequent efforts have illuminated several extant challenges:
 83 a relatively limited number of unambiguously temperature-sensitive chronolo-
 84 gies, a predominance of ring-width chronologies in comparison to the more
 85 temperature-sensitive wood density measurements (D’Arrigo et al., 1992; Schwe-
 86 ingruber et al., 1993; Briffa et al., 2004; Frank et al., 2007; D’Arrigo et al., 2009;
 87 Esper et al., 2015; Wilson et al., 2016), and the influence of non-stationarity in
 88 climate/tree growth associations (‘divergence’; Briffa et al., 1998b; Wilson et al.,
 89 2007; D’Arrigo et al., 2008), a particular problem for North American treeline
 90 tree-ring width chronologies (Jacoby and D’Arrigo, 1995; Andreu-Hayles et al.,
 91 2011; Anchukaitis et al., 2013) and many previously collected wood density
 92 chronologies (Briffa et al., 2002). Since the publication of D’Arrigo et al. (2006)
 93 and Wilson et al. (2007), dozens of new tree-ring chronologies and local temper-
 94 ature reconstructions have become available, including many new and updated
 95 latewood density (MXD) measurement series that do not appear to exhibit any
 96 divergence (c.f. D’Arrigo et al., 2009; Esper et al., 2010; Anchukaitis et al.,
 97 2013). We draw on these new, published, and updated data here to develop a
 98 spatial reconstruction of past summer temperature stretching back to 750 CE.
 99 This work extends the non-spatial hemisphere mean reconstruction published
 100 by Wilson et al. (2016).

101 Methodologies for last millennium climate reconstructions have been exten-
 102 sively investigated and tested over the last two decades (Mann and Rutherford,
 103 2002; Rutherford et al., 2003; Zorita et al., 2003; von Storch et al., 2004; Esper
 104 et al., 2005; Mann et al., 2005; Smerdon et al., 2008; Lee et al., 2008; Smer-
 105 don et al., 2010; Mann et al., 2007; Li et al., 2010; Smerdon et al., 2011; Wang
 106 et al., 2015; Smerdon and Pollack, 2016). However, neither reduced space, em-
 107 pirical orthogonal regression methods (c.f. Fritts, 1991; Cook et al., 1994; Mann
 108 et al., 1998) nor most variants of regularized expectation maximization (RegEM

109 Schneider, 2001; Rutherford et al., 2003; Mann et al., 2009) explicitly consider
 110 the location of the proxies relative to the reconstruction target, and therefore
 111 reconstructions of individual grid points can be significantly influenced by dis-
 112 tant proxy sites. While there is potential value in taking into account large-scale
 113 teleconnections between the climate in a remote region and the local conditions
 114 controlling proxy formation (Evans et al., 2001, 2002), the potential disadvan-
 115 tage to these approaches is that they rely implicitly on the existence, stability,
 116 and persistence of those teleconnections (Gershunov and Barnett, 1998; Rimbu
 117 et al., 2003; Anchukaitis et al., 2006; Wilson et al., 2010; Lehner et al., 2012;
 118 Gallant et al., 2013; Ortega et al., 2015; Wise, 2015; Lewis and LeGrande, 2015),
 119 assume the time-stability of large-scale covariance patterns, and risk admitting
 120 distal predictors with spurious relationships to local temperatures. However,
 121 several methods exist which do account for the spatial distribution and rela-
 122 tionship of the proxy predictor network to the target field (Cook et al., 1999;
 123 Tingley and Huybers, 2010; Steiger et al., 2014). Here we use Point-by-Point
 124 regression (PPR; Cook et al., 1999) to develop, for the first time, a hemisphere-
 125 scale spatial temperature reconstruction. For an extensive review of the full
 126 range of climate field reconstruction methods, see Tingley et al. (2012).

127 We seek a spatial reconstruction of past temperatures that utilizes a predic-
 128 tor network with a clear biophysical and statistical relationship with temper-
 129 ature. We therefore apply the expert knowledge of the original developers of
 130 the individual chronologies and reconstructions, relying on their experience with
 131 respect to climate signal evaluation and statistical treatment (c.f. Esper et al.,
 132 2016). PPR is a well-established, transparent, and spatially-explicit methodol-
 133 ogy for climate field reconstruction. The result of PPR here is a gridded map of
 134 summer temperature anomalies for each year of the last ~ 1200 years with asso-
 135 ciated validation skill metrics in both space and time. An additional benefit of
 136 PPR is that limiting the grid point reconstructions to proximal predictors and
 137 avoiding assumptions about the global covariance structure ensures that distant
 138 grid points remain independent of one another. The spatial features of the field
 139 can therefore be examined and compared without concern that they arise from

140 use of the same predictors.

141 We compare our results against radiative forcing over the last millennium
142 (Schmidt et al., 2012), diagnosing the potential role of volcanic eruptions and
143 insolation variability in shaping the Northern Hemisphere extratropical warm
144 season temperature response across space and time. Our field reconstruction
145 can serve as a resource for understanding temperature variability in the past,
146 for comparison with other proxy records of environmental and climate change,
147 and to provide context for coupled human-natural systems response to climate
148 variability (e.g. Buckley et al., 2010; Büntgen et al., 2011; Pederson et al., 2014;
149 Büntgen et al., 2016). Our reconstruction also provides a spatiotemporal target
150 appropriate for formal detection and attribution of the influence of different
151 sources of radiative forcing on the Earth’s climate system.

152 2. Materials and Methods

153 2.1. Tree-ring series

154 Tree-ring based reconstructions of large-scale climate variability, whether a
155 single mean time series or a spatial climate field reconstruction, require selecting
156 potential proxy predictors from the many thousands of chronologies that have
157 been developed over the last century of tree-ring research (St. George, 2014).
158 The majority of these chronologies were not collected or developed with the
159 intended purpose of temperature reconstruction and do not contain a primary
160 temperature signal. It is therefore necessary to apply some selection procedure,
161 lest chronologies lacking temperature information overwhelm the predictor set
162 with ‘noise’ associated with soil moisture, archaeological selection, ecological
163 processes, or spurious non-temperature signals. Two broad categories of ap-
164 proach have been used for initial predictor selection: statistical screening and
165 expert assessment. In statistical screening (c.f. Mann et al., 2008), proxy se-
166 ries are assessed for their correlations against local or regional observational
167 temperature data, with those data passing some significance, sign, or effect
168 size threshold then admitted to the pool of potential predictors. While this

169 approach clearly has merit as an objective and automated approach, it virtu-
 170 ally guarantees the selection of a proportion of proxies without a realistic bio-
 171 physical or substantial statistical association with the climate variable targeted
 172 for reconstruction. A second approach utilizes expert assessment of individual
 173 chronologies based on an understanding of whether a proxy has the requisite
 174 ecological, biological, geographical, and climatological characteristics to serve
 175 as a reasonable temperature proxy. Although this approach is not completely
 176 isolated from statistical considerations, the advantage is that it strongly reduces
 177 the likelihood that a non-temperature proxy or nonsense predictor will enter into
 178 a temperature reconstruction model. Expert assessment can include not only
 179 climate signal and ecological criteria, but also the methods used to develop the
 180 proxy series (e.g. Esper et al., 2016). A potential disadvantage to this approach
 181 is that it is partially subjective and therefore different investigators could make
 182 different selections for the predictor pool. Hybrid approaches that combine sim-
 183 ple mechanistic or physiological assessment with statistical evaluation have also
 184 been applied (c.f. Tierney et al., 2015).

185 Here, we follow Wilson et al. (2016) and use as our predictor series only pub-
 186 lished tree-ring chronologies and temperature reconstructions that demonstrate
 187 an established and biophysically reasonable association with local temperatures.
 188 These include both tree-ring chronologies as well as existing temperature recon-
 189 structions from Northern Hemisphere high-latitude and high-altitude locations,
 190 where dendrochronological and ecological principles suggest the most limiting
 191 factor for growth is temperature (Fritts, 1976). We exclude from considera-
 192 tion chronologies south of 40°N to avoid confounding climate signals associated
 193 with moisture-sensitive trees (St. George, 2014) and we also reject chronologies
 194 known to demonstrate evidence of the ‘divergence problem’ (Briffa et al., 1998b;
 195 D’Arrigo et al., 2008, 2009; Wilson et al., 2007), a problem previously observed
 196 to affect North American *Picea glauca* tree-ring width chronologies (D’Arrigo
 197 et al., 1992, 2009; Andreu-Hayles et al., 2011; Esper et al., 2012) and many
 198 MXD chronologies developed in the 1970s and 1980s. We require that our pre-
 199 dictors extend back to at least 1750 CE and completely forward to 1988 CE.

200 The predictors retain the detrending and standardization choices of the original
 201 authors. The resulting dataset is designated N-TREND2015 and is composed
 202 of a mixture of tree-ring width (TRW), MXD (Schweingruber et al., 1978), and
 203 blue intensity (BI; McCarroll et al., 2002) data. N-TREND2015 is archived and
 204 publicly available¹ and is the same dataset used in Part 1 of this study (Wilson
 205 et al., 2016). N-TREND is intended to be a ‘living dataset’ that will grow or
 206 be modified as new proxies become available or are updated. Details of the
 207 predictor time series used here and in Wilson et al. (2016) are available in Table
 208 1. As shown in Figure 1, the NTREND-2015 network reflects a mix of proxy
 209 types, dominated by MXD or BI (43 series, vs. 11 composed of tree-ring width
 210 data only). A total of 54 series are available from 1750 to 1988 CE, the time
 211 period of full (denoted ‘BEST’) coverage of the network. The number of sites
 212 drops precipitously toward the present, down to 34 by 1990 CE and to 25 series
 213 by 2000 CE, with only 3 sites remaining by 2011. There are 23 series at 1000
 214 CE and 4 remain at 750 CE, the limits of our reconstruction. While all the
 215 tree-ring chronologies and reconstructions have significant and substantial cor-
 216 relations with local temperatures in one or more months, locations that include
 217 MXD and BI data overall have higher correlations compared to sites composed
 218 of tree-ring width data alone (Figure 2; see also Wilson et al. (2016)).

219 *2.2. Observational data*

220 Our target field (predictand) for our temperature reconstruction is the inter-
 221 polated hybrid (surface and satellite information) version of HadCRUT4 from
 222 Cowtan and Way (2014). The original HadCRUT4 (Morice et al., 2012) con-
 223 sists of monthly temperature anomalies relative to the mean of the 1961 to 1990
 224 CE period on a regular 5° latitude/longitude grid and combines CRUTEM4
 225 (Jones et al., 2012) over land with HADSST3 (Kennedy et al., 2011a,b) for the
 226 oceans. Use of the Cowtan and Way (2014) dataset provides several advantages
 227 here: First, this dataset seeks to compensate for observational coverage bias

¹https://www.ncdc.noaa.gov/cdo/f?p=519:1:0:::P1_study_id:19743

and provides gridded estimates of monthly temperature at high latitudes, including portions of our target reconstruction region north of 40°N . Second, it is spatially and temporally complete, allowing us to use the same calibration and validation periods for our reconstruction at every location in the field, which in turn permits straightforward comparisons of reconstruction skill. Following Wilson et al. (2016), we use May through August (MJJA) mean temperature anomalies as our target variable, as this season provides a network-wide balance across the diverse site-local monthly or seasonal climate responses of the individual predictor series (Wilson et al., 2016).

2.3. Reconstruction and statistical methodology

As a prelude to our climate field reconstruction, we assess the spatial characteristics of the temperature signal across our network. We first calculate the Pearson Product Moment correlation between each series and the local gridded MJJA temperatures from Cowtan and Way (2014) as a measure of the correspondence between tree growth and local gridded temperatures. We also calculate, for each site, the field correlation between the individual predictor series and the entire MJJA and annual mean temperature field, using both the original data as well as first-differenced series. For assessing the association between the target field and the predictor network, we follow Schneider et al. (2015) and compute the median correlation coefficient between the temperature record at each grid box and all the predictor times series within 2000 km of the centroid (see below; Briffa and Jones, 1993; Jones et al., 1997; Cook et al., 2013). We perform this procedure for both the best replicated part of our predictor network (1750 to 1988 CE) and at 1000 CE in the midst of the Medieval epoch. Collectively, these statistical assessments provide an evaluation of the climate signal embedded in the predictor network through time and space.

We use Point-by-Point Regression (PPR; Cook et al., 1999) to reconstruct the MJJA surface temperature anomaly field north of 40°N using our predictor network of tree-ring proxy chronologies and temperature reconstructions. We follow the method as developed, tested, and described by Cook et al. (1999,

258 2010a, 2013). PPR incorporates the spatial structure of the predictor network
259 and predictand field and confines the potential region of influence of the pre-
260 dictors to a distance estimated from the underlying correlation structure of the
261 temperature field. PPR proceeds by calculating a nested multivariate regression
262 model for each grid point in the target field with the predictors restricted to
263 those within some radius from the grid point centroid. We adopted a dynamic
264 search radius for each grid point in the target field, first identifying predictor
265 series within 1000km. If no chronologies were found within 1000km, the radius
266 was allowed to expand in 500km increments up to a maximum of 2000km to find
267 predictors. These distances are based on the decorrelation decay as a function of
268 distance in the target field data (Cowtan and Way, 2014) and are also consistent
269 with the findings of other studies (Briffa and Jones, 1993; Jones et al., 1997;
270 Cook et al., 2013). If no predictors were found within 2000km, then no climate
271 reconstruction was produced for that grid point. In evaluating our methods,
272 we found that this dynamic search radius provides an optimal balance between
273 maximizing the number of grid points available for reconstruction while allowing
274 the local predictor series in data-dense regions (for instance, Fennoscandia and
275 western Europe) to provide the paleoclimate information for their neighborhood
276 of grid points.

277 A multivariate regression model was calibrated for each grid point and its
278 associated predictors over the period 1945 to 1988 CE (the latest date for which
279 all chronologies had data) and then validated on withheld observational data
280 over the period 1901 to 1944 CE (Michaelson, 1987). We also checked the sen-
281 sitivity of our reconstruction to this choice of calibration and validation periods
282 by swapping them and assessing cross-validation. As the number of predictor
283 series declines back through time, the model is newly calibrated and validated at
284 each change in sample depth. In our reconstruction, we use the individual series
285 themselves as predictors as opposed to the leading principal components (PCs).
286 In our sensitivity tests of the PPR method, we discovered that using PCs from
287 a relatively sparse network of chronologies and reconstructions, combined with
288 the expansive target field, created clearly artificial inhomogeneities or disconti-

289 nities when predictor numbers declined. Using the individual predictor time
 290 series themselves in a stepwise regression model with an adjusted R^2 entry rule
 291 (Meko, 1997) ameliorated such discontinuities. Model skill was assessed using
 292 the calibration R_c^2 (adjusted for the number of predictors), the validation R_v^2 ,
 293 the Reduction of Error (RE) and the Coefficient of Efficiency (CE) (c.f. Cook
 294 et al., 1999; Wilson et al., 2006). In addition to the annual maps of reconstructed
 295 temperatures, we calculate an extratropical Northern Hemisphere mean MJJA
 296 time series using a latitude weighted average of all the reconstructed grid cells
 297 where reconstructed values are available back to at least 1000CE and RE is
 298 greater than zero.

299 Following Masson-Delmotte et al. (2013), we calculated the difference be-
 300 tween reconstructed Medieval Climate Anomaly (MCA) and Little Ice Age
 301 (LIA) temperatures by taking the difference between the mean values over the
 302 field for 950 to 1250 CE (MCA) and 1450 to 1850 CE (LIA). As there is no single
 303 accepted definition of these two periods (Hughes and Diaz, 1994; Bradley et al.,
 304 2001; Matthews and Briffa, 2005; Seager et al., 2008; Mann et al., 2009), we
 305 also tested the sensitivity of the calculated MCA-LIA to differences in the time
 306 definition of these periods. We estimated the temperature response to tropical
 307 explosive volcanism (Robock, 2000; Ammann and Naveau, 2003) by calculating
 308 the composite mean anomaly using superposed epoch analysis (e.g. Haurwitz
 309 and Brier, 1981). Event years were extracted from most recent updated esti-
 310 mates of Common Era volcanic forcing from Sigl et al. (2015), here selecting
 311 those years corresponding to an estimated maximum negative event forcing (in
 312 Wm^{-2}) with a magnitude at least as large as Krakatoa in 1883.

313 **3. Results**

314 *3.1. Network climate signal*

315 All our predictor series show significant and typically high correlations with
 316 local summer temperatures over one or several months (Figure 2, 3; Wilson
 317 et al. (2016)). At sites where the highest local summer temperature signal

318 in the series is confined to one or two months – for example, at Yakutia in
 319 Russia – local correlations with the broader MJJA season are lower ($r = 0.52$,
 320 $p < 0.05$ for July vs. $r = 0.09$, $p > 0.05$ for MJJA at Yakutia). The highest
 321 individual monthly/seasonal site local temperature correlations (Wilson et al.,
 322 2016) range from $r = 0.39$ to $r = 0.84$ (mean $r = 0.63$), while correlations with
 323 local MJJA temperatures range from $r = 0.04$ to $r = 0.78$ (mean $r = 0.43$).
 324 The highest correlations with local MJJA temperatures are in Fennoscandia
 325 and north central Russia, with strong local temperature signals also evident in
 326 Scotland, the Alps, the Pyrenees, the Altai, and Japan. In North America, MXD
 327 chronologies from western Canada and the northern treeline have the strongest
 328 MJJA signals. Tree-ring width only chronologies in North America have a
 329 generally weaker association with their local MJJA instrumental temperature
 330 than MXD or mixed proxy sites (D’Arrigo et al., 1992; Jacoby and D’Arrigo,
 331 1995; D’Arrigo et al., 2009; Andreu-Hayles et al., 2011; Anchukaitis et al., 2013).

332 Field correlations between the predictor series and the full MJJA tempera-
 333 ture field (Figure 4) suggest that the chronologies and temperature reconstruc-
 334 tions reflect climate variability over many hundred or thousands of kilometers,
 335 with some exceptions at those sites where the local proxy response to MJJA is
 336 already weak (e.g. locations in east Asia, Yakutia, and ring width-only chronolo-
 337 gies from the North American treeline). The spatial extent of the large-scale
 338 correlation structure is partially related to the common positive trends in predic-
 339 tors and temperatures during the 20th century, as temporarily removing these
 340 trends by first differencing both the field and the predictors (Figure 5) reduces
 341 the regions of positive correlations to between 500 and 2000 kilometers. In
 342 some case – e.g. the Idaho (USA) chronology – a significant interannual corre-
 343 lation with the MJJA temperature field is entirely absent, indicating the sum-
 344 mer association there is driven by common trends and a narrow local monthly
 345 temperature response. Annual temperatures are often a target for tempera-
 346 ture reconstruction (e.g. Esper et al., 2002; D’Arrigo et al., 2006; Mann et al.,
 347 2008, 2009); however, correlations with the annual temperature field herein are
 348 uniformly lower and many chronologies show no significant association with an-

349 nual mean temperatures (Figure 6). In general, higher correlations with annual
 350 mean temperatures are observed for those sites with higher local correlations
 351 with MJJA temperatures ($r_{MJJA,annual} = 0.73$, $p < 0.01$). The association
 352 between the annual signal and the best (highest) monthly or seasonal local cli-
 353 mate correlations is weaker ($r_{best,annual} = 0.44$, $p < 0.01$), indicating it is not
 354 a strong climate signal *alone* that corresponds with a useful *annual* proxy, but
 355 rather a strong *and* broad seasonal climate response.

356 Figure 7 shows the statistical relationships between the predictand target
 357 field and predictor network. Grid points in Asia, Fennoscandia, and Northern
 358 Europe have 15 or more proxy sites that can serve as predictors over the best
 359 replicated epoch (1750 to 1988 CE). In northwestern North America as many as
 360 10 predictors are within 2000km of the grid centroids. In contrast, grid points in
 361 southern Europe and eastern North America have many fewer predictors avail-
 362 able, in some cases only a single series. For the best replicated portion of the
 363 reconstruction, 1750 to 1988 CE, the median correlation between observational
 364 MJJA temperatures at each grid point and the predictors within 2000km of
 365 that grid point range from $r = -0.19$ in northeastern Russia to $r = 0.66$ in
 366 Fennoscandia. In general, the median grid correlations are highest where they
 367 are co-located with one or more chronologies (e.g. interior British Columbia)
 368 and regions with clusters of strong MJJA temperature proxies (e.g. Fennoscan-
 369 dia, the Alps and Pyrenees, northern North American treeline). By 1000 CE,
 370 when the number of predictors is reduced to 23, with only 3 of these in North
 371 America, the possible reconstruction domain is reduced as substantially fewer
 372 predictors are available for each grid point reconstruction. Nevertheless, grid
 373 median correlations between observed temperatures and the available predictors
 374 remain significant and of similar magnitude to the better replicated recent por-
 375 tion of the reconstruction. This is because predictors with strong temperature
 376 signals remain in the Alps, Icefields in British Columbia, the Gulf of Alaska,
 377 Fennoscandia, northern Russia, and the Altai. The reconstruction at 1000 CE
 378 and earlier therefore relies on a reduced number of predictors, but those that
 379 remain contain a significant and substantial temperature signal.

3.2. Field reconstruction, calibration, and validation

The full NTREND spatial reconstruction consists of 1239 yearly fields of MJJA temperature anomalies covering up to a potential 792 grid points each year (40 to 90°N, -180 to 180°E). Figure 8 shows the length of the reconstructed temperature series at each grid point in our domain. In practice the number of grid points with a value in each year of the reconstruction is less than that potential maximum, as the full network can only support reconstruction at 85% ($n = 701$) of the total grid cells in the domain, declining to 51% ($n = 401$) by 1000 CE and 24% ($n = 190$) by 750 CE. The shortest reconstructions are for ocean grid points in the northwestern Atlantic and northeastern Pacific, where in both cases a single and relatively short chronology is the only source of proxy information. Other relatively short portions of the field reconstruction include the central northern treeline in Canada, Japan, northeastern Russia, and the southernmost part of the Eurasian domain in the Mediterranean. By contrast, along the Eurasian treeline in central northern Russia, throughout the Nordic region, and in western Europe, it is possible to reconstruct more than a millennium of past temperatures.

Figure 9 shows reconstruction skill (the adjusted R_c^2 , R_v^2 , RE , and CE) for the best replicated ($n = 54$) period of the predictor network, 1750 to 1988 CE. Significant skill is observed over the entire domain, but is clearly highest closest to those predictors with the highest correlations to MJJA temperatures, especially where MXD or BI data are available. Grid cells more distal from the predictor network, including cells over the oceans, or where only a single or relatively weak predictor is available, show lower explained variance and in some cases lack positive RE and CE scores. Validation R_v^2 scores are lower but largely mirror the calibration R_c^2 , with the exception of the eastern Mediterranean and Black Sea region, east Asia, and western parts of Central Asia. A similar phenomenon of lower R_v^2 was observed by Cook et al. (2013) for Asia, due at least in part to the lack of instrumental climate data from these regions during the reconstruction model validation period (Jones et al., 2012; Harris et al., 2013; Cook et al., 2013; Cowtan and Way, 2014). Lack of instrumental data

likely confounds out-of-sample validation in the eastern Mediterranean prior to the 1930s (c.f. Touchan et al., 2014). Skillful regions with RE and CE scores greater than 0 are more spatially confined but likewise show skill with respect to these metrics in regions where chronologies are present or abundant, with the exception once again of the regions mentioned previously. R_c^2 values range from ~ 0.0 to 0.78, R_v^2 values range from ~ 0.0 to 0.76, RE up to 0.72, and CE up to 0.70. A cross-validation (not shown) interchanging the time periods used for calibration and validation reveals that the reconstruction’s skill characteristics are largely insensitive to the choice of these periods.

By 1000 CE, the reduction in the number of predictors and a contraction in their spatial distribution influences both the number of grid points reconstructed and the spatial patterns of skill (Figure 10). The loss of the northern treeline MXD chronologies in North America reduces the reconstructed regions of the continent in the west to coastal Alaska, the Pacific Northwest, Interior British Columbia and parts of Alberta, and in the east to Quebec, Newfoundland, and Labrador. Likewise, the loss of the Scottish and Pyrenees chronologies no longer allow for reconstruction of temperatures over the British Isles and the Iberian peninsula. The lack of Japanese, coastal Russia, and east Asia series at 1000 CE leads to a contraction of the reconstructed spatial domain in the east. However, skillful temperature reconstructions persist over parts of northwestern North America, Fennoscandia, northern Russia, the Alps, and the Altai. R_c^2 values range from ~ 0.0 to 0.73, R_v^2 values range from ~ 0.0 to 0.70, RE up to 0.65, and CE up to 0.61. Interchanging the calibration and validation periods has a minor influence on field skill at 1000 CE, with $n = 229$ grid points with $RE > 0$ for a late calibration (1945 to 1988 CE), and $n = 213$ for an early calibration (1901 to 1944 CE).

Figure 11 shows domain-wide reconstruction and skill metrics over time. For the time span of the full predictor network (1750 to 1988 CE), we can reconstruct a temperature anomaly value for 88.5% of the grid points ($n = 701$) in our extratropical Northern Hemisphere domain. Of those 701 grid points, 63% have $RE > 0$, and 37% have $CE > 0$. These skill percentages remain

442 remarkably stable (RE , 56% to 65%; CE , 34% to 37%) even as the number
 443 of reconstructed grid points with a reconstructed value declines back through
 444 time, a consequence of the shrinking predictor network. Only when the number
 445 of reconstructed grid points declines precipitously in the earliest 10th century,
 446 falling to 38% of the target domain in 905 CE, do the percent of grid points with
 447 RE and CE greater than zero *increase* substantially. These patterns indicate
 448 that the reduction in the number of reconstructed grid cells comes at the cost
 449 of locations with already marginal skill scores, while the core reconstruction
 450 regions associated with sensitive predictor series persist through much of the
 451 length of the reconstruction back to 750 CE.

452 3.3. Large-scale mean temperature anomalies and climate forcing

453 We computed a mean summer temperature anomaly series from our domain
 454 by calculating a latitude-weighted mean of all gridded values where a reconstruc-
 455 tion is available back to 1000CE and RE is greater than zero (Figure 12). This
 456 time series is highly and significantly correlated with the comparable observa-
 457 tional temperature anomalies averaged over those same grid points (1850–1988,
 458 $n = 139$, $r = 0.78$, $p < 0.001$). The mean series indicates a broad warm
 459 period from at least 750 CE to the early 1400s, with maximum values centered
 460 around the late 900s, the late 1000s and 1100s, and the individual warmest years
 461 of the Medieval epoch in 790, 990, 995, 1014, 1016, and 1168 CE. 1168 CE is
 462 the warmest year in our reconstruction (750 to 1988 CE), although matched by
 463 values in the middle of the 20th century and then exceeded during the compara-
 464 ble filtered instrumental record in the early 21st century. Temperatures decline
 465 in the late 13th century, coincident with a series of tropical volcanic eruptions
 466 (Crowley, 2000; Gao et al., 2008; Schmidt et al., 2012; Sigl et al., 2015) and the
 467 Wolf solar irradiance minimum, before warming again during the 14th century.
 468 Temperatures then decline sharply in the early 1400s, slightly before the signif-
 469 icant volcanic eruptions in the 1450s (Gao et al., 2006; Sigl et al., 2015) and the
 470 Spörer solar irradiance minimum (1460 to 1550 CE). The mid-1400s through the
 471 mid-1800s show cooler conditions during the LIA (Matthews and Briffa, 2005;

472 Masson-Delmotte et al., 2013), with local minima in the 1450s, the late 1500s
 473 and earliest 1600s, the late 1600s, and the early 1800s. Many of the field-mean
 474 coldest years in the reconstruction, including 1259, 1453, 1601, 1643, 1783, 1810,
 475 1817, and 1836 CE are associated with or follow closely after major tropical or
 476 Northern Hemisphere volcanic eruptions (Briffa et al., 1998a; Sigl et al., 2015).
 477 In several instances extremely cold years in our reconstruction occur or persist
 478 at least one or two years after eruptions (e.g. 1643 and 1644, 1816 and 1817,
 479 1836 and 1837 CE), consistent with the findings of Esper et al. (2013b). The
 480 coldest year in our reconstruction is 1601 CE, which also agrees with a prior
 481 temperature reconstruction based solely on MXD data by Briffa et al. (1998a),
 482 and which follows the eruption of Huaynaputina in Peru in 1600 CE (Verosub
 483 and Lippman, 2008). Our ten coldest years include at least 2 (1699 and 1867
 484 CE) that do not appear to be associated with a known volcanic eruption (Briffa
 485 et al., 1998a).

486 Our filtered time series is highly and significantly correlated (750–1988 CE,
 487 $n = 1239$, $r = 0.71$, $p < 0.01$) with the index reconstruction from Wilson
 488 et al. (2016) and perhaps unsurprisingly has many of the same features - a
 489 broad warm period during the Medieval until the early 1400s, the LIA from
 490 the 15th through early 19th century, warming out of the LIA, a warm mid-
 491 20th century, cool 1970s, and recent warming (Figure 13a). There are epochs
 492 where our mean time series and that of Wilson et al. (2016) are less strongly
 493 correlated (Figure 13b); interestingly, the rapid returns to higher correlation
 494 values appear to be associated with the timing of major individual or clusters of
 495 volcanic events, suggesting that strong radiative forcing due to volcanism may
 496 impose a common spatial forcing, causing the Wilson et al. (2016) mean index
 497 reconstruction and the spatial mean from our climate field reconstruction to
 498 converge.

499 Our Northern Hemisphere extratropical time series shows associations with
 500 large-scale radiative forcing changes during the last millennium (Figure 14;
 501 Schmidt et al., 2012). Colder periods in the late 13th and early 14th, mid-15th,
 502 and 19th century occur at the same time as large explosive volcanic eruptions

503 and solar minima (Mann et al., 1998; Crowley, 2000; Shindell et al., 2001a, 2003;
 504 Wagner and Zorita, 2005; Ammann et al., 2007; Breitenmoser et al., 2012; An-
 505 chukaitis et al., 2013; PAGES2k, 2013). Warming after the middle of the 19th
 506 century is consistent with a reduced number of volcanic eruptions, increasing
 507 insolation, and the rapid rise in greenhouse gases (Andronova and Schlesinger,
 508 2000; Zwiers and Weaver, 2000; Gillett et al., 2012; Jones et al., 2013; Estrada
 509 et al., 2013). Although the timing of several epochs of colder temperatures ap-
 510 pear to align with solar minima – for instance, the late 13th/early 14th century
 511 and the Wolf Minumum or the mid-15th century Spörer Minimum – the corre-
 512 lations between our hemisphere mean reconstruction and estimates of past solar
 513 variability (Schmidt et al., 2012) are low (range, $r = 0.10$ to $r = 0.29$, $p < 0.01$).
 514 At centennial timescales, however, there is evidence that solar variability may
 515 play a more substantial role. Wavelet coherence (Figure 15; Grinsted et al.,
 516 2004) between our hemisphere mean reconstruction and last millennium total
 517 solar irradiance estimates assembled by Schmidt et al. (2012) shows high and
 518 stable coherence and consistent phasing at bi-centennial time scales (194 to 222
 519 year periods), which bracket and include the ~ 206 year ‘de Vries’ (or Suess)
 520 solar cycle (Stuiver and Braziunas, 1993; Wagner et al., 2001) and are likely
 521 related to the reconstructed temperature response to the major solar minima.
 522 The spectral signal of the bicentennial de Vries cycle has been recognized in nu-
 523 merous tree-ring chronologies and temperature reconstructions (c.f. Raspopov
 524 et al., 2008; Breitenmoser et al., 2012; Ogurtsov et al., 2016), and Emile-Geay
 525 et al. (2013) also identified bi-centennial periodicity in a reconstruction of east-
 526 ern tropical Pacific sea surface temperatures. Phase relationships between our
 527 hemisphere mean temperature and the total solar irradiance time series suggest
 528 a decadal-scale lag of ~ 11 years (range, 5 to 20 years), with solar changes lead-
 529 ing temperature anomalies, consistent with both climate modeling and prior
 530 analysis of tree-ring chronologies and solar variability (Rind et al., 1999; Waple
 531 et al., 2002; Breitenmoser et al., 2012). Both the hemisphere mean as well as
 532 the spatial grid point sensitivity to solar variability (C/Wm^{-2}) are extremely
 533 uncertain in this analysis, however, as this quantity is highly sensitive to the

choice of solar reconstruction (Schmidt et al., 2012).

Medieval Climate Anomaly (MCA; 950 to 1250 CE) temperatures compared against those during the Little Ice Age (LIA; 1450 to 1850 CE) show warmer temperature during the MCA at $\sim 90\%$ of the grid points with minimally skillful ($RE > 0$) reconstructed values available back to 950 CE (Figure 16). Colder Medieval temperatures are reconstructed over parts of the Altai and Central Asia, and are associated with tree-ring width chronologies from Mongolia that show reduced growth in the 900s and 1100s, despite warmer conditions in the 11th century (Davi et al., 2015) and an MXD chronology from the Altai displaying a cold Medieval epoch and warm LIA (Schneider et al., 2015). Other grid cells that show a colder Medieval period tend to be distal from the predictor network – for instance in central Greenland – and must be treated with caution. Defining a different MCA or LIA in this case has relatively little effect on the percentage of grids showing warmer vs. colder conditions, as the cooler Central Asia grid cells and marginal cells in Greenland, central Canada, the southern Caspian Sea, and the northeastern Pacific remain irrespective of the specific date range applied. The precise boundaries for both MCA and LIA are, in any case, both arbitrary and uncertain (Hughes and Diaz, 1994; Bradley et al., 2001; Matthews and Briffa, 2005; Seager et al., 2008). The cause of apparently extremely high ($\sim 3^\circ\text{C}$) Medieval temperatures in several grid points in northeastern North America is discussed below.

Composite mean MJJA temperature anomaly fields following major volcanic eruptions show coherent, broad-scale cooling associated with large tropical eruptions (Figure 17). 96% of grid points show composite mean colder temperatures compared to the three years prior to the 20 large eruptions considered here. Similar to the MCA-LIA difference discussed above, regions that apparently have an overall composite warming response to volcanic eruptions are largely on the margins of the reconstruction domain, away from the predictor grid, and over the ocean, central Greenland, and the southern Caspian Sea. The coldest grid point composite mean is -1.61°C , and the mean composite response across all grid points and all eruptions is -0.44°C . Closer examination of indi-

vidual eruption events (not shown) finds that for some regions, post-volcanic cooling may persist for several years and maximum cold anomalies may be 1 or 2 years after the year of the eruption itself, consistent with observations of other regional temperature reconstructions (D’Arrigo et al., 2013; Cook et al., 2013; Esper et al., 2013b; Davi et al., 2015; Linderholm et al., 2015; Schneider et al., 2015; Wilson et al., 2016). If we consider large Northern Hemisphere high-latitude eruptions only (Figure 18), the large-scale response is likewise toward cold anomalies overall: 89% of grid points have a composite anomaly less than zero. Over the entire field the mean composite response is -0.39°C and the maximum cold composite anomaly is -2.31°C . There is also spatial structure to the temperature anomalies, with the coldest composite conditions over Alaska and the Bering Strait, northeastern North America, parts of western Europe, and central northern Russia, suggestive of a dynamical, in addition to direct radiative, influence of large-magnitude high latitude eruptions (Robock, 2000; Oman et al., 2005; Stenchikov et al., 2006; Schneider et al., 2009; Zanchettin et al., 2012; Pausata et al., 2015). However, the number of radiatively significant high latitude eruptions considered here is smaller ($n = 5$), and therefore this structure may appear due to the limited sample size.

4. Discussion

4.1. Proxy data and predictor network

Our results here demonstrate that a relatively small ($n = 54$) network of proxy sites (Table 1, Figure 1) with well-established physically and ecologically reasonable climate signals (Figure 3, 7) can be used to reconstruct the large-scale summer temperature history of the extratropical Northern Hemisphere (Figure 8, 9, 10, 12). While restricting the reconstruction to the higher latitudes of one hemisphere and to only the growing season does not provide a global annual estimate of temperature, it nonetheless accurately reflects the geographic and biological signal that dominates the predictors. Moreover, we have demonstrated here that the reconstruction preserves the signature and influence of external

594 forcing on the global energy balance. Skill in our reconstruction is, perhaps not
 595 surprisingly, greatest in those locations where high quality temperature-sensitive
 596 proxies are available (Figure 9, 10), and declines at increasing distances from
 597 the predictors themselves. It is clear we could realize substantial benefits in
 598 terms of increased reconstruction skill and spatial extent by developing MXD
 599 and BI chronologies from currently undersampled regions as well as extending
 600 the length of existing MXD and BI chronologies. Although large and useful
 601 multiproxy datasets have resulted from community efforts by the paleoclimate
 602 community (PAGES2k, 2013), our analysis here demonstrates that a relatively
 603 small well-distributed network of highly sensitive millennium-length tree ring
 604 chronologies provide skillful reconstructions over a large extratropical region.
 605 Encouragingly, this means that rapid and important gains could be made from
 606 the addition of a relatively small number of new sites and the temporal exten-
 607 sion and recollection of current sites known to contain a strong climate signal.
 608 In particular, a greater number of long MXD and BI chronologies are critically
 609 needed from North America (Figures 1, 10). Fulfilling this need will require a
 610 collaborative and concerted effort to locate subfossil materials and to measure
 611 density proxies, but the potential gain for Northern Hemisphere temperature
 612 reconstructions of the Common Era would be substantial. MXD contains a
 613 stronger temperature signal than TRW alone and is better able to accurately
 614 resolve rapid temperature changes associated with volcanic eruptions (Figure
 615 2; Frank et al., 2007; D’Arrigo et al., 2013; Esper et al., 2015). Continuing
 616 advances in blue intensity (BI) measurements suggest some of the benefits of
 617 wood density analysis can be realized without the expense and difficulty of an-
 618 alyzing MXD itself (Campbell et al., 2007; Wilson et al., 2014; Rydval et al.,
 619 2014; Björklund et al., 2014; Björklund et al., 2015) although the low-frequency
 620 characteristics of BI still requires additional exploration.

621 Detrending and standardization issues for long chronologies remain an ongo-
 622 ing challenge and persistent source of uncertainty (e.g. Cook et al., 1995; Briffa
 623 and Melvin, 2011; Melvin and Briffa, 2008; Esper et al., 2012; Matskovsky and
 624 Helama, 2014; Esper et al., 2016; Matskovsky and Helama, 2016). One surpris-

ing feature of the epochal comparison between the MCA and LIA is the large
 ($> 3^{\circ}\text{C}$) difference calculated for northeastern North America. This feature is
 due to a single predictor, a black spruce (*Picea mariana*) tree-ring width RCS
 chronology developed by Gennaretti et al. (2014). Other, non-tree ring proxies
 from the region suggest a lower amplitude of cooling between the MCA and the
 LIA, although issues related to time uncertainty, transfer function calibration,
 and different seasonal climate signals complicate exact comparisons. A com-
 pilation of Holocene paleoenvironmental data for the Arctic (Sundqvist et al.,
 2014) suggests a range of values for MCA to LIA cooling in northeastern North
 America and Greenland of 0 to 1.5°C , which is at least a degree less than the
 magnitude inferred from the Quebec MXD record. Alkenone SST reconstruc-
 tions near Nova Scotia (Keigwin et al., 2003) suggest a cooling of approximately
 0.7°C . The multiproxy PAGES Arctic2k reconstruction (McKay and Kaufman,
 2014) has a whole-Arctic reconstructed MCA-LIA difference of 0.64°C for the
 same time periods used here. Finally, and perhaps most importantly, a tree-
 ring oxygen isotope temperature reconstruction from the same site in Quebec
 (Naulier et al., 2015) shows a substantially smaller estimated MCA-LIA differ-
 ence of 0.4°C . It seems likely that, despite the care taken in applying regional
 curve standardization to the Quebec black spruce samples (Autin et al., 2015)
 as well as its suitability with respect to other chronology metrics (Esper et al.,
 2016), artifacts remain in this tree-ring width chronology that unintentionally
 but artificially amplify the difference between MCA and LIA temperatures in
 this region.

More generally, detrending, the removal of non-climatic trends, and there-
 fore the retention of low frequency variability, remains an important source
 of uncertainty in the amplitude of past temperatures reconstructed from tree
 rings (Cook, 1987; Briffa et al., 1996), even when conservative detrending tech-
 niques have been applied. While regional curve standardization and signal free
 methods have been shown to be able to retain the full spectrum of low- and
 medium-frequency variability, they are also subject to their own uncertainties
 and assumptions (Melvin, 2004; Melvin and Briffa, 2008; Briffa and Melvin,

2011; Anchukaitis et al., 2013; Briffa et al., 2013). It is in most cases not possible to know from calibration and validation statistics which detrending method yields the true or most accurate low frequency signal (Cook, 1987; Cook and Kairiūkštis, 1990; Wilson et al., 2007). Possible approaches to this problem include both ensemble and simulation-based methods (e.g. Esper et al., 2007; D’Arrigo et al., 2011; Anchukaitis et al., 2013), although these have not yet been applied to large and heterogeneous tree-ring proxy networks.

4.2. Radiative forcing and temperature history

Our reconstruction demonstrates coherent responses to radiative forcing in time and space (Figures 14, 15, 16, 17, 18). Temporal features of the reconstruction are associated with changes in solar irradiance, large and/or clustered tropical volcanic eruptions, and the anthropogenic rise in well-mixed greenhouse gases. Temperatures decline across the field during the Spörer and Maunder Minima, in particular, likely compounded in both cases by a series of volcanic eruptions. Temperatures remained cold during the early 1600s, at least in part due to the eruption of Huaynaputina in Peru in 1600 CE (Verosub and Lippman, 2008). 1601 CE is the coldest year of our entire reconstruction, as it was in the 600 year temperature reconstruction by Briffa et al. (1998a) and the hemisphere mean reconstruction by Wilson et al. (2016). 1601 CE was also one of the coldest years in the Bayesian field reconstruction by Tingley and Huybers (2013), as was 1453 CE, which is the 4th coldest year in our study, associated with the eruption of of Kuwae, Vanuatu (but see Plummer et al., 2012; Cole-Dai et al., 2013). Interestingly, Tingley and Huybers (2013) find 1642 CE amongst their coldest years, whereas in our reconstruction it is 1643 CE that is exceptionally cold (5th coldest in our reconstruction). In Wilson et al. (2016), 1641, 1642, and 1643 CE are all amongst the coldest 15 years of their reconstruction. Tingley and Huybers (2013) also find that 1695 CE was anomalously cold, whereas here it is indeed cold but unremarkable (-0.60°C , 284th coldest). These differences highlight extant uncertainties likely related to different reconstruction methods, spatial skill and averaging, and the use of different proxies (D’Arrigo et al.,

2013; Esper et al., 2015), but also demonstrate that there is no evidence for a one-to-one correspondence between inferred volcanic forcing from ice cores and the magnitude of hemisphere-scale cooling. For instance, the eruption of Huaynaputina in 1600 is believed to have caused a smaller negative radiative forcing anomaly than eruptions in 1458, 1641, 1809, and 1815 CE, let alone the large Medieval eruption of Samalas (1257 CE) (Verosub and Lippman, 2008; Lavigne et al., 2013; Sigl et al., 2015). Our finding here of a large-scale, coherent cooling in response to explosive volcanism is yet further evidence (Anchukaitis et al., 2012; Brohan et al., 2012; D’Arrigo et al., 2013; Esper et al., 2013b,a; St. George et al., 2013; Büntgen et al., 2014; Jull et al., 2014; Esper et al., 2015; Sigl et al., 2015; Stoffel et al., 2015; Wilson et al., 2016) against the hypothesis that tree-ring proxies are missing the volcanic cooling signal due to undetected absent rings (Mann et al., 2012, 2013).

Low frequency coherence between solar variability and our reconstruction appears to be a stable characteristic through time (Figure 14, 15), likely linked to reconstructed cold anomalies during solar Grand Minima. Because variations in total solar irradiance are relatively small, on the order of a few tenths of a Wm^{-2} , the mechanism that could result in a detectable cooling remains uncertain. The most likely connection is via changes in large-scale Northern Hemisphere circulation, which favor colder temperature over continents (e.g. Shindell et al., 2001a, 2003; Swingedouw et al., 2010) and thus would be captured in our reconstruction. Nevertheless, while variability in solar forcing may be important on bicentennial and perhaps at continental scales, fingerprinting suggests that the solar effect in the hemisphere-scale anomalies is otherwise relatively small and that volcanic forcing is more important overall in determining pre-industrial temperature trajectories (Schurer et al., 2014; McGregor et al., 2015). There is no sign in our reconstruction of a discernible temperature response to the shorter 11 and 22 year sunspot cycle (Schwabe/Hale), which is consistent with other investigations of the insolation signal in tree rings (e.g. Briffa, 1994). There are a number of possible reasons for the absence of this signal: Internal climate system variability is substantially stronger at interannual

and decadal time scales, which may prevent statistical detection of solar influences with similar frequencies, but still allow it at the centennial scale when the magnitude of internal variability is smaller than the forced signal. Short-term climate anomalies caused by explosive volcanism could also disrupt detection of a decadal solar signal. The temperature response to solar variability at lower frequencies may also reflect slow temperature feedbacks that enhance its direct effect.

Over those grid points available back to 950 CE with minimum level of reconstruction skill ($RE > 0$), $\sim 90\%$ show warmer conditions during the MCA than during the LIA, with a field median difference of 0.32°C . Removing likely individual grid point outliers (Greenland and northeastern North America, see above) results in a slightly smaller epochal field median difference (0.30°C) and a range of grid point values of -0.64 to $+1.05^\circ\text{C}$. Mann et al. (2009) calculated a 0.24°C global summer mean difference between MCA and LIA, but the difference in season, spatial domain and geographic extent, and the ‘fragility’ (Wang et al., 2015) of reconstructing a cold Medieval tropical Pacific make any direct comparison difficult. Calculating the MCA-LIA epochal difference using the spatial mean time series (Figure 12) gives a value of 0.36°C , approximately in the middle of the distribution for other large-scale Northern Hemisphere reconstructions, and within the higher end of the range of values from climate model simulations (Fernández-Donado et al., 2013; Wilson et al., 2016).

5. Conclusions and future work

We have reconstructed the extratropical Northern Hemisphere MJJA temperature anomaly field back to 750 CE using a network of temperature-sensitive predictors. The reconstruction shows significant field skill associated with proximity to the predictors, particularly where proxy density data are available. In other words, we observe the most reconstruction skill and smallest errors where we have the most sensitive tree-ring proxies, whereas higher errors and lower skill are associated with grid points distal from the predictor network or where only

tree-ring width data are available, particularly in North America. These observations will be used to guide future sampling and proxy development priorities, including the development of new sites, efforts to increase the number of MXD and BI series, and the extension in time of existing high quality chronologies.

Our field reconstruction reveals coherent responses to changes in radiative forcing over the last 1200 years, including the influence of solar and volcanic forcing. Future research with our field reconstruction will use fingerprint detection (Hegerl et al., 2007; Schurer et al., 2013, 2014) to quantitatively assess the role of forcing and internal variability, including identification of spatial patterns linked to large-scale modes of variability and specific forcing agents. Formal, quantitative comparison between our reconstruction and paleoclimate model simulations (Schmidt et al., 2012; Kageyama et al., 2016) will be used to assess climate model performance and to investigate the dynamical context for reconstructed spatial temperature anomalies. Using proxy system models (Evans et al., 2013), the NTREND network could also be applied within an offline data assimilation framework (Steiger et al., 2014; Hakim et al., 2016). Finally, our spatially-explicit reconstructions can be used to explore and understanding the possible role of past temperature variability – especially volcanic eruptions – in contributing to historical societal dynamics, resilience, and change (McCormick et al., 2007; Ludlow et al., 2013; Sigl et al., 2015; Büntgen et al., 2016)

Acknowledgements

The N-TREND consortium is not itself funded, but many individuals acknowledge relevant projects, grants, and support; KJA: National Science Foundation Paleoclimate Perspectives on Climate Change NSF AGS-1501856 and NSF AGS-1501834; RW: UK Natural Environment Research Council (NERC - NE/K003097/1) and Leverhulme Trust project (F/00 268/BG); KRB and TO: NERC (Belmont Forum/JPI-Climate: INTEGRATE project NE/P006809/1); KRB also thanks Gaurav Kapur FRCR and Colin Watts FRCS for time; UB: Czech project ‘Building up a multidisciplinary scientific team focused on drought’

775 No. CZ.1.07/2.3.00/20.0248; EC: National Science Foundation Paleoclimate
776 Perspectives on Climate Change AGS-1502224; RD: National Science Founda-
777 tion Paleoclimate Perspectives on Climate Change AGS-1159430, AGS-1502150,
778 and AGS-1502224; SH: Academy of Finland; GH and AS: ERC advanced grant
779 TITAN (EC-320691), NCAS GH specifically with a Royal Society Wolfson Re-
780 search Merit Award (WM130060); GH and AS: PACMEDY, NE/P006752/1;
781 HL: The Swedish Science Council (VR) (2012-5246); MR: The Carnegie Trust
782 for the Universities of Scotland; GW: NSF AGS-1502186. The N-TREND
783 project website, along with the archived TR chronologies and temperature re-
784 constructions can be found at [https://www.ncdc.noaa.gov/cdo/f?p=519:1:](https://www.ncdc.noaa.gov/cdo/f?p=519:1:0:::P1_study_id:19743)
785 [0:::P1_study_id:19743](https://www.ncdc.noaa.gov/cdo/f?p=519:1:0:::P1_study_id:19743) and additional information is available at [https:](https://ntrenddendro.wordpress.com/)
786 [//ntrenddendro.wordpress.com/](https://ntrenddendro.wordpress.com/). Lamont-Doherty Earth Observatory con-
787 tribution #####.

Table 1: Tree-ring chronology and temperature reconstruction predictor series used in the reconstruction. Additional information is available in Wilson et al. (2016). Latitude is given in degrees North, and longitude is in degrees East. A range of latitude/longitude indicates the data or reconstruction cover a larger region. Detrending: STD: traditional detrending standardization; RCS: regional curve standardization; SF: signal free extension to STD or RCS standardization. † indicates series used in D’Arrigo et al. (2006) and ‡ those used in Wilson et al. (2007)

Site Name	Code	Latitude	Longitude	Time Span	Proxy Type	Detrending	Citation
NORTH AMERICA							
Seward	NTR	65.11 to 65.22	-162.18 to -162.27	1710-2001	MXD	STD	D’Arrigo et al., 2004
Coastal Alaska	GOA	60.01 to 60.45	-149.31 to -141.42	800-2010	TRW	RCS	Wiles et al., 2014
Wrangells	WRAX	60-65	-145.00 to -140.00	1593-1992	MXD	STD	Davi et al., 2003 ‡
Firth	FIRT	68.39	-141.38	1073 - 2002	MXD	RCS-SF	Anchukaitis et al. 2013
Southern Yukon	YUS	59 to 62	-140 to -133	1684-2000	TRW	STD	Youngblut and Luckman, 2008 ‡
Northern Yukon	YUN	65 to 70	-125 to -135	1638-1988	TRW	STD	Szeicz and MacDonald, 1995 †
Int. British Columbia	IBC	49.02 to 50.59	-121.43 to -117.03	1600-1995	TRW/MXD/BI	STD/SF	Wilson et al., 2014
Icefields	ICE	52.16	-117.19	918 - 1994	RW/MXD	RCS	Luckman and Wilson, 2005 †
Idaho	IDA	40 to 45	-110 to -120	1135-1992	TRW	STD	Biondi et al., 1999 ‡
Coppermine	COP	67.14	-115.55	1551 - 2003	MXD	STD	D’Arrigo et al. 2009, Anchukaitis et al. 2013
Thelon	THE	64.02	-103.52	1492 - 2004	MXD	STD	D’Arrigo et al. 2009, Anchukaitis et al. 2013
Quebec	QUEX	57.30	-76.00	1373-1988	MXD	RCS	Schneider et al. 2015
Quebec	QUEW	57.30	-74.00	910-2011	TRW	RCS	Gennaretti et al., 2014
Northern Quebec	NQU	55 to 60	-70 to -65	1642-2002	TRW	STD	Payette, 2007 ‡
Labrador	LABREC	56.33 to 57.58	-62.25 to -61.56	1710-1998	TRW/MXD	STD/RCS	D’Arrigo et al., 2003, 2013
EURASIA							
Scotland	SCOT	57.08	-3.44	1200-2010	TRW/BI	STD/RCS	Rydval et al. in review
Pyrenees	PYR	42 to 43	0 to 1	1260-2005	MXD	RCS	Dorado-Liñán et al., 2012
W Alps - Lentschental	ALPS	46.5	9	755-2004	MXD	RCS	Büntgen et al., 2006
E Alps - Tyrol	TYR	47.30	12.30	1053-2003	MXD	RCS	Schneider et al. 2015
Jaemland	JAEM	63.30	13.25	783-2011	MXD	RCS	Zhang et al., 2016
Tjeggelvas, Arjeplog, & Ammanäs composite	TAA	65.54 to 66.36	16.06 to 18.12	1200-2010	MXD	RCS	Linderholm et al., 2015
North Fennoscandia	EFmean	66 to 69	19 to 32	750-2010	MXD	RCS	Esper et al., 2014, Matskovsky and Helama, 2014
Forfjordalen	FORF	68.47	15.43	978-2005	MXD		McCarroll et al., 2013
Tatra	TAT	48 to 49	19 to 20	1040-2010	TRW	RCS	Büntgen et al., 2013
Mt Olympus, Greece	MOG	40.09	22.37	1521-2010	MXD	RCS	Klesse et al., 2015
South Finland	SFIN	62.19	28.19	760-2000	MXD	RCS	Helama et al., 2014
Khibiny (Kola)	KOL	67.38 to 67.50	33.13 to 34.15	821-2005	RW/BI	RCS/STD	McCarroll et al., 2013
Polar Urals	POLx	66.51	65.40	891-2006	MXD	RCS	Schneider et al. 2015
Yamal	YAM	67.32	69.54	750-2005	TRW	RCS-SF	Briffa et al., 2013
Asia Grid 1	Grid1	40.15 to 46.15	60.15 to 68.15	817-1989	mix	RCS/STD	Cook et al., 2013
Asia Grid 2	Grid2	40.15 to 46.15	70.15 to 78.15	827-1989	mix	RCS/STD	Cook et al., 2013
Asia Grid 10	Grid10	48.15 to 54.15	60.15 to 68.15	937-1989	mix	RCS/STD	Cook et al., 2013
Asia Grid 11	Grid11	48.15 to 54.15	70.15 to 78.15	937-1989	mix	RCS/STD	Cook et al., 2013
Kyrgyzstan	KYR	41.36 to 42.11	75.09 to 78.11	1689-1995	TRW/MXD	STD	Wilson et al., 2007 ‡
Mangazeya	MAN	66.42	82.18	1328-1990	MXD	RCS	Schneider et al. 2015
Asia Grid 3	Grid3	40.15 to 46.15	80.15 to 88.15	800-1989	mix	RCS/STD	Cook et al., 2013
Asia Grid 12	Grid12	48.15 to 54.15	80.15 to 88.15	800-1989	mix	RCS/STD	Cook et al., 2013
Altai MXD	ALT	50.00	88.00	750-2007	MXD	RCS	Schneider et al. 2015
Asia Grid 4	Grid4	40.15 to 46.15	90.15 to 98.15	800-1989	mix	RCS/STD	Cook et al., 2013
Asia Grid 13	Grid13	48.15 to 54.15	90.15 to 98.15	1024-1989	mix	RCS/STD	Cook et al., 2013
Mongolia	OZN	51.15	99.04	931-2005	TRW	RCS	Davi et al., 2015
Taymir	TAY	72.01	102.00	755-1997	TRW	RCS	Jacoby et al., 2000 †
Asia Grid 5	Grid5	40.15 to 46.15	100.15 to 108.15	800-1989	mix	RCS/STD	Cook et al., 2013
Asia Grid 14	Grid14	48.15 to 54.15	100.15 to 108.15	1396-1989	mix	RCS/STD	Cook et al., 2013
Asia Grid 6	Grid6	40.15 to 46.15	110.15 to 118.15	800-1989	mix	RCS/STD	Cook et al., 2013
Asia Grid 15	Grid15	48.15 to 54.15	110.15 to 118.15	1396-1989	mix	RCS/STD	Cook et al., 2013
Asia Grid 7	Grid7	40.15 to 46.15	120.15 to 128.15	1024-1989	mix	RCS/STD	Cook et al., 2013
Asia Grid 16	Grid16	48.15 to 54.15	120.15 to 128.15	1510-1989	mix	RCS/STD	Cook et al., 2013
Asia Grid 8	Grid8	40.15 to 46.15	130.15 to 138.15	1510-1989	mix	RCS/STD	Cook et al., 2013
Asia Grid 17	Grid17	48.15 to 54.15	130.15 to 138.15	1510-1989	mix	RCS/STD	Cook et al., 2013
Asia Grid 9	Grid9	40.15 to 46.15	140.15 to 148.15	1510-1989	mix	RCS/STD	Cook et al., 2013
Asia Grid 18	Grid18	48.15 to 54.15	140.15 to 148.15	1510-1989	mix	RCS/STD	Cook et al., 2013
North Japan	NJAP	43 to 51	142 to 145	1640-1993	TRW/MXD	STD	D’Arrigo et al., 2015
Yakutia	YAK	67.27 to 70.33	142.37 to 150.17	1342-1994	TRW	RCS	Hughes et al., 1999 †

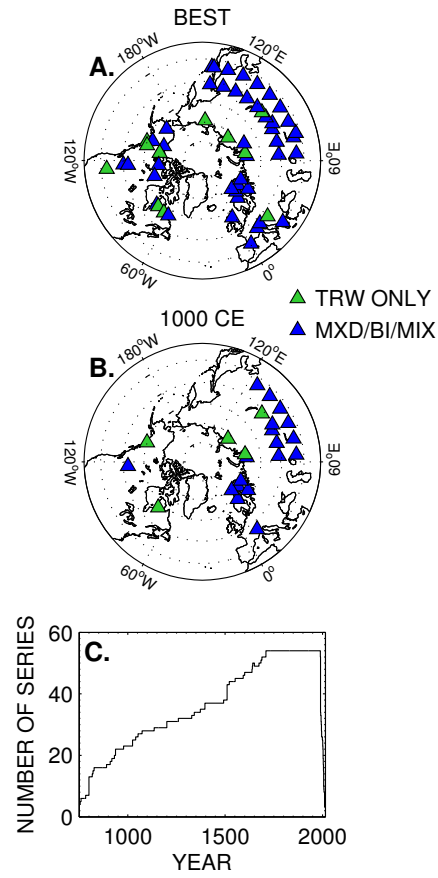


Figure 1: Spatial and temporal distribution of sites by proxy type. Top panel (A) shows all the records available during the best replicated (most recent, 1750 to 1988 CE) nest, while the bottom panel (B) shows the distribution of available proxy sites at 1000 CE. Sites with tree-ring width (TRW) data only are shown in green, while sites that have MXD, BI, or a mix of proxy types are shown in blue. (C) Shows the total number of series through time.

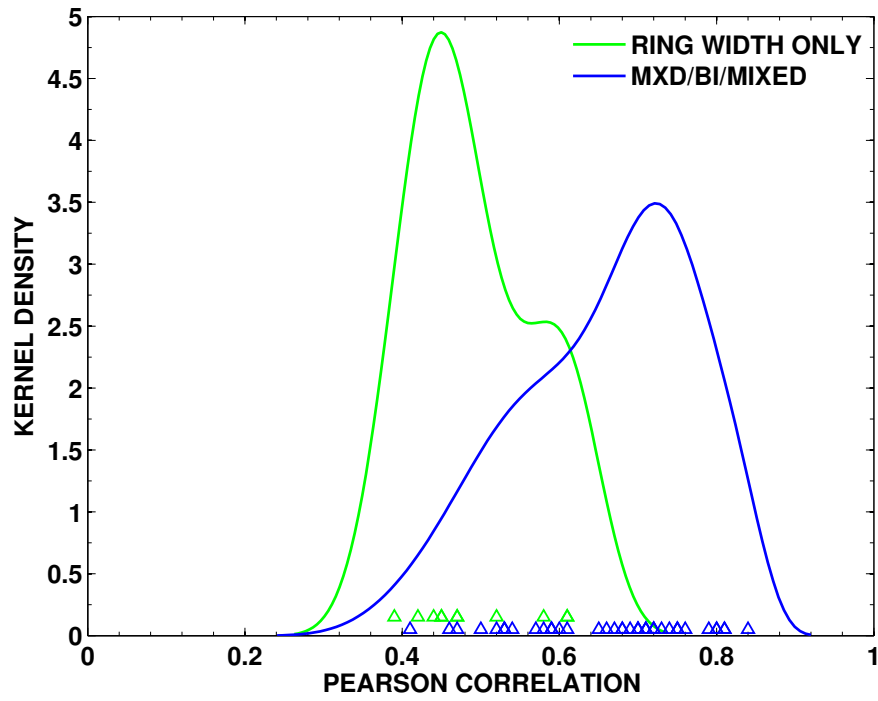


Figure 2: Kernel probability density estimate (Bowman and Azzalini, 1997) for the highest local seasonal or monthly coefficient correlations as a function of proxy type. Data are from Wilson et al. (2016)). The density estimate is calculated for a support of $[-1,1]$ and the values contributing to the distribution are indicated by symbols along the x-axis.

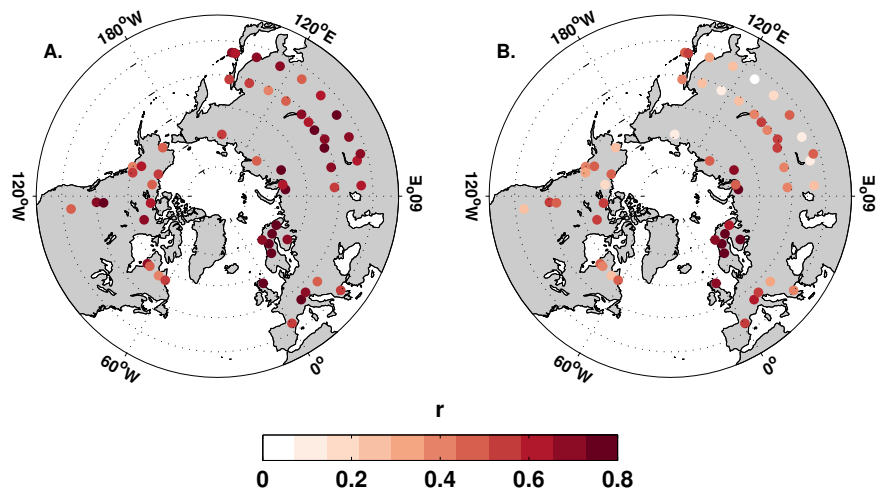


Figure 3: Local correlations between tree-ring proxy chronologies and local temperature data. (A) Correlations reported by the original authors for local correlations with the optimal seasonal or monthly window (see Wilson et al., 2016, their Table 1). (B) Correlations between each proxy series and the local May through August (MJJA) temperature data from Cowtan and Way (2014) used here.

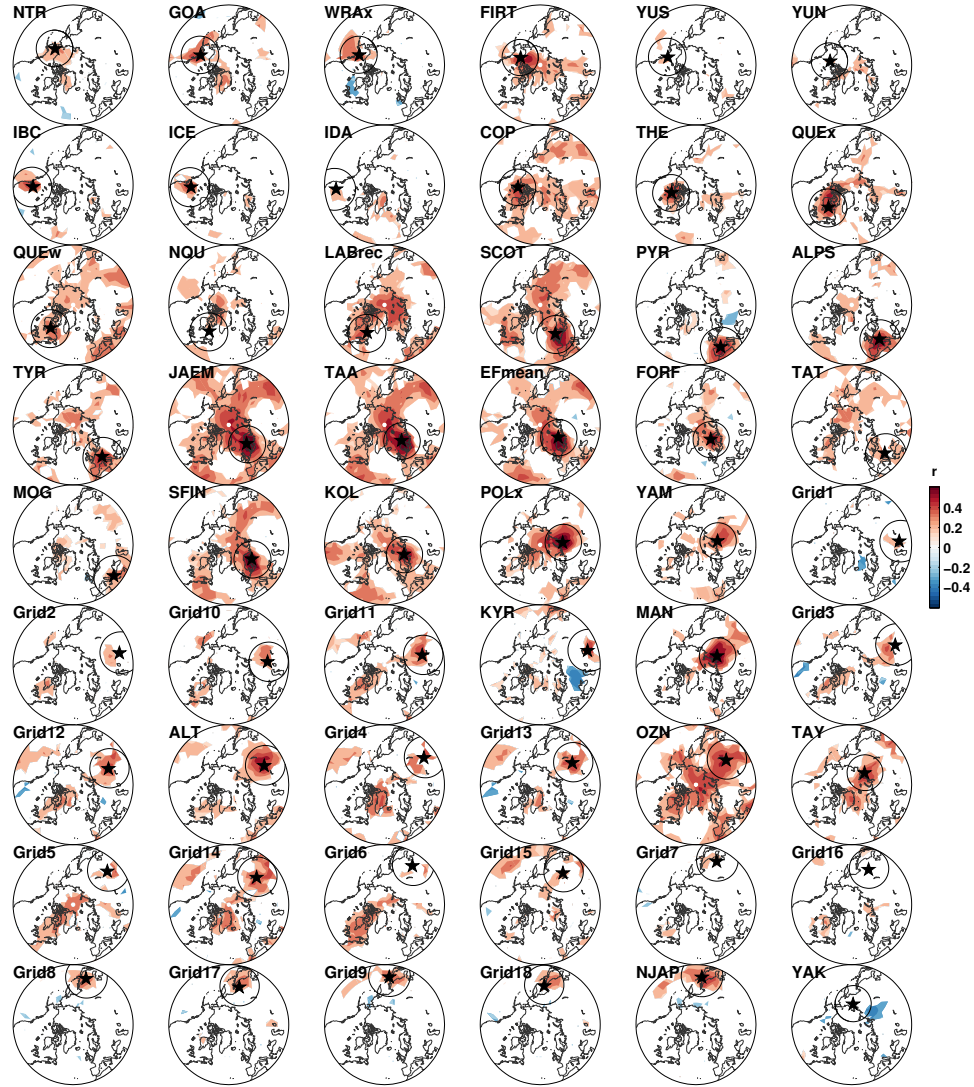


Figure 4: Field correlations between each tree-ring site (indicated by the black stars) and the MJJA mean temperature field from Cowtan and Way (2014). Labels correspond with the site codes from Table 1. Around each site the black range ring indicates a radii of 2000 km. Only Pearson Product Moment correlation coefficients (r) significant at $p < 0.05$ as adjusted for autocorrelation (Trenberth, 1984) are plotted.

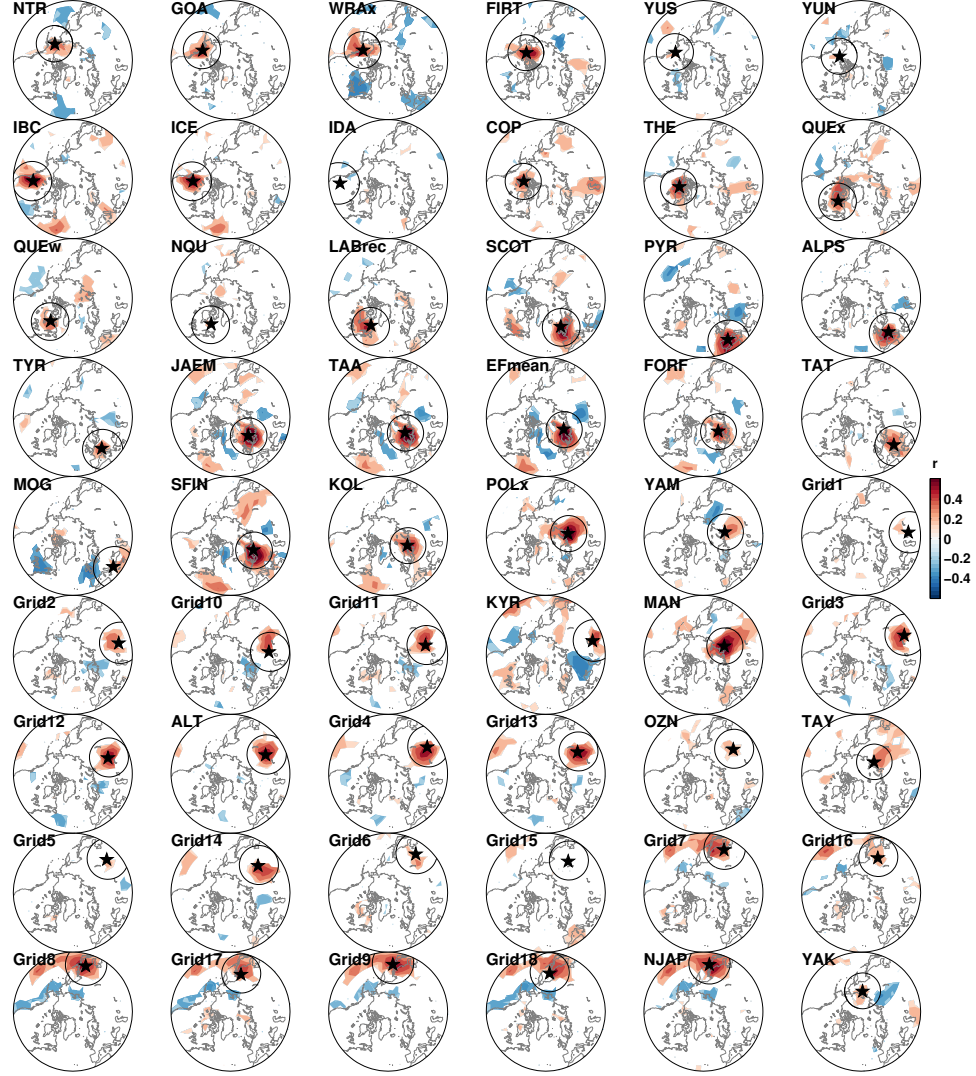


Figure 5: Field correlations between each tree-ring site (indicated by the black stars) and the MJJA mean temperature field from Cowtan and Way (2014) after first-differencing each variable to reduce the influence of common trends. Labels correspond with the site codes from Table 1. Around each site the black range ring indicates a radii of 2000 km. Only Pearson Product Moment correlation coefficients (r) significant at $p < 0.05$ as adjusted for autocorrelation (Trenberth, 1984) are plotted.

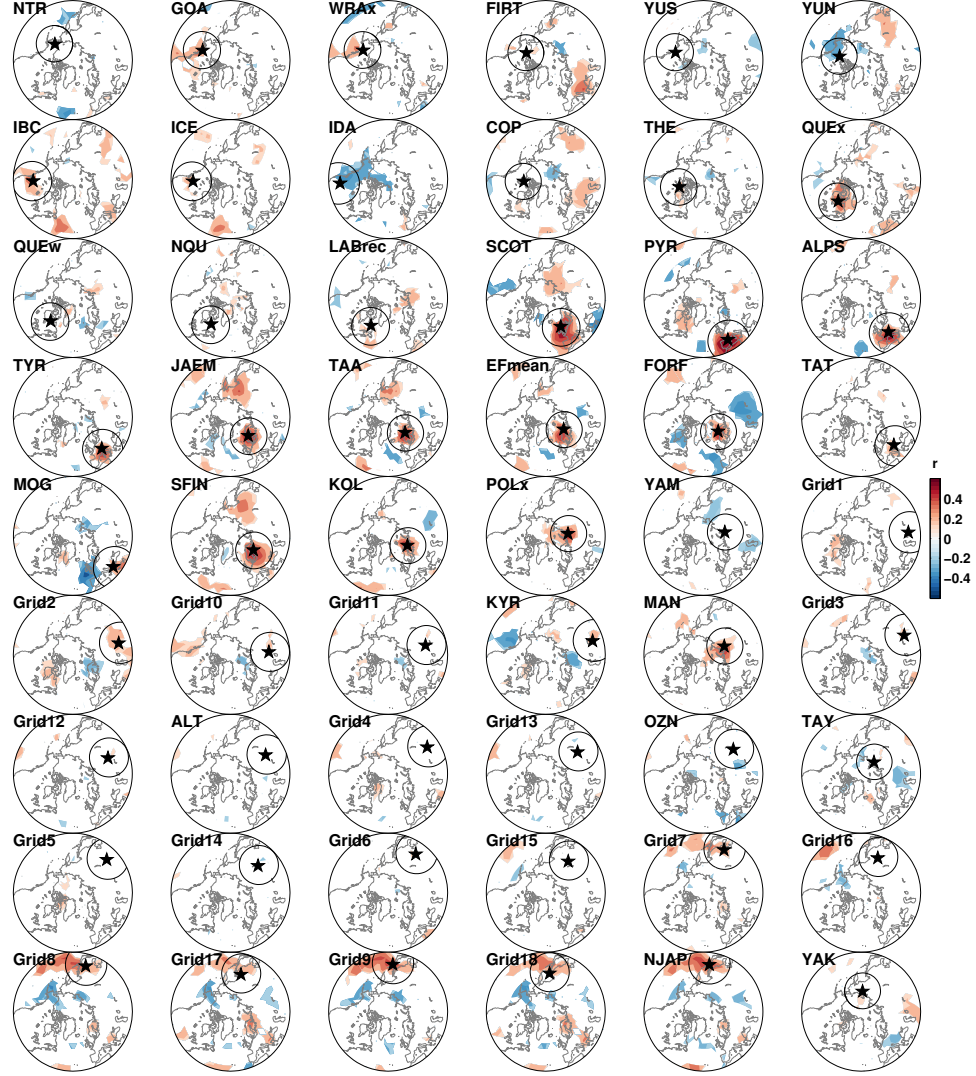


Figure 6: Field correlations between each tree-ring site (indicated by the black stars) and the annual mean temperature field from Cowtan and Way (2014) after first-differencing each variable to reduce the influence of common trends. Labels correspond with the site codes from Table 1. Around each site the black range ring indicates a radii of 2000 km. Only Pearson Product Moment correlation coefficients (r) significant at $p < 0.05$ as adjusted for autocorrelation (Trenberth, 1984) are plotted.

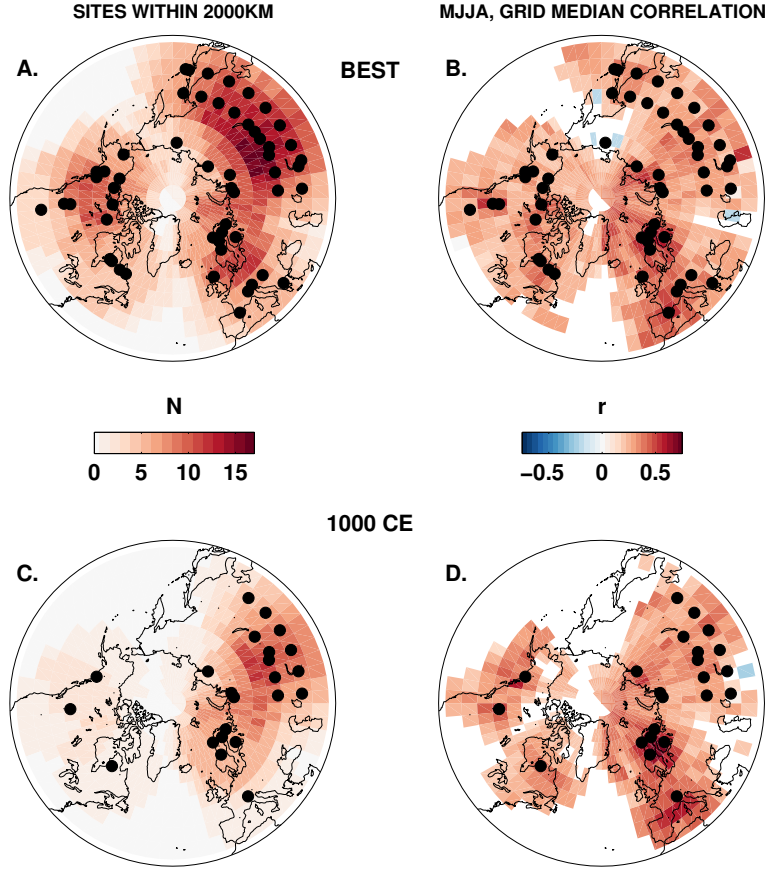


Figure 7: Proxy and target grid characteristics. Panels (A) and (C) show the number of tree-ring sites within 2000km for each grid point in the target field (Cowtan and Way, 2014), during the best replicated (modern) nest (A) and at 1000 CE (C), respectively. Black circles indicate the location of the available tree-ring sites during in each time period. Panels (B) and (D) show the median value at each target field grid point for the Pearson Product Moment correlation between the MJJA temperatures at that grid point and all the tree-ring chronologies within 2000km of that grid, during the best replicated (modern) nest (B) and at 1000 CE (D), respectively (see Schneider et al. (2015)).

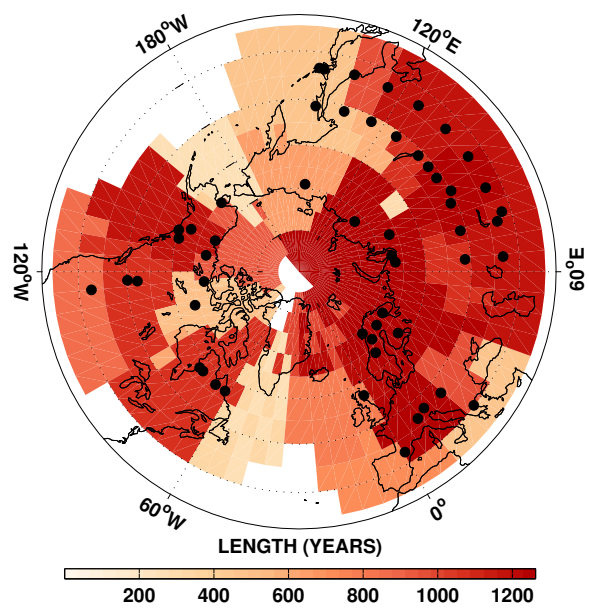


Figure 8: Reconstruction length. The length (in years) of the reconstruction at each target grid point.

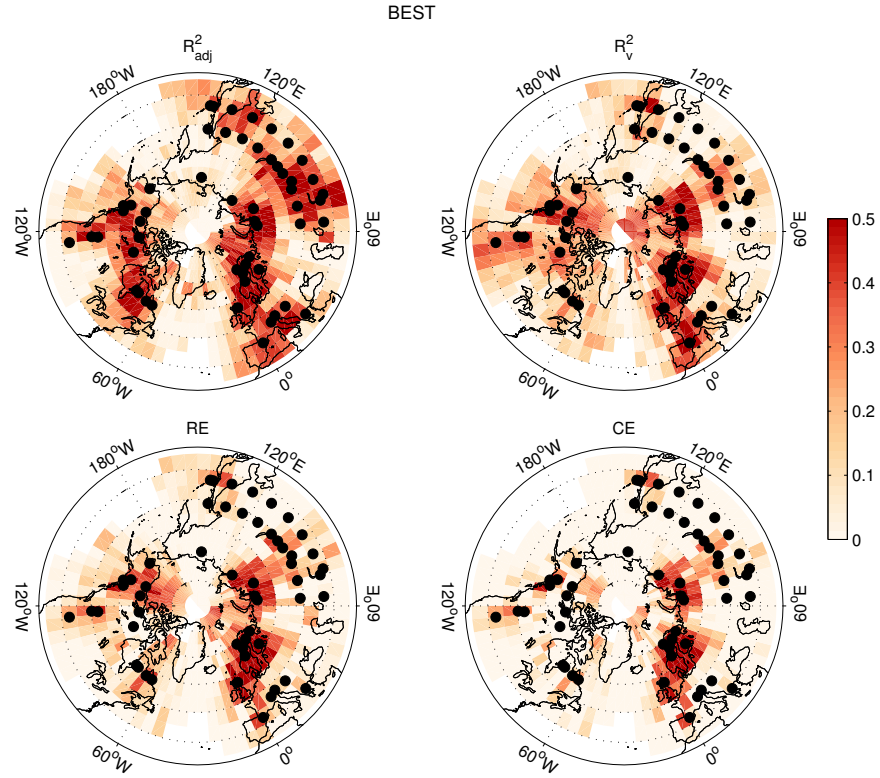


Figure 9: Reconstruction skill for the best replicated (modern) nest. Panels show spatial patterns of skill metrics for the best replicated nest (1750 to 1988 CE), as evaluated for the adjusted calibration R^2 , the validation R^2 , the reduction of error (RE), and the coefficient of efficiency (CE). Available tree-ring sites during this nest are indicated by black circles.

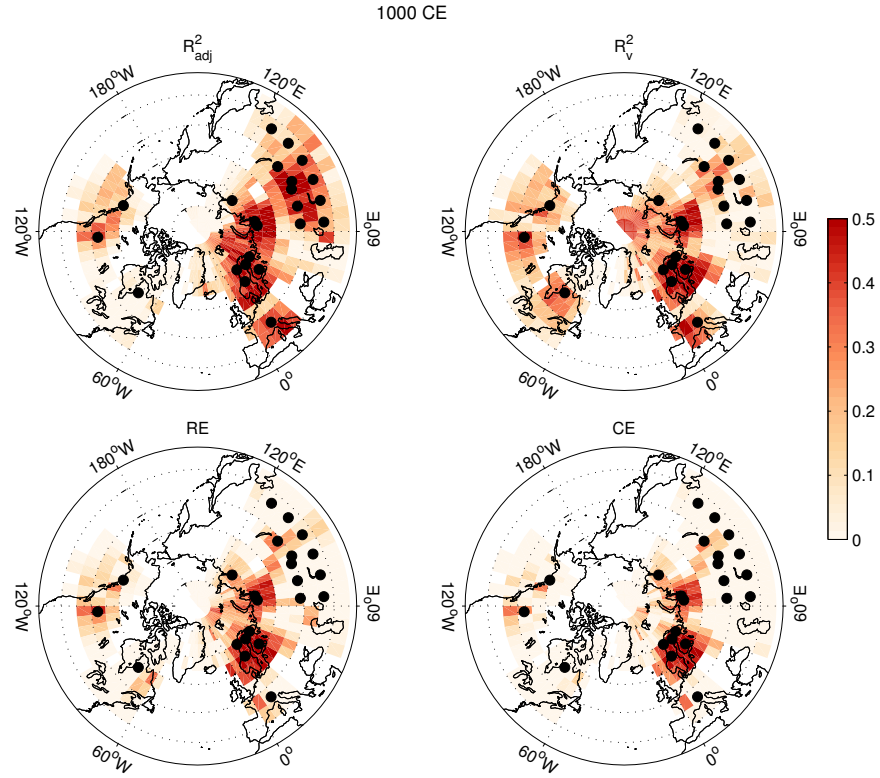


Figure 10: Reconstruction skill at 1000 CE. Panels show spatial patterns of skill metrics for the reconstructed field at 1000 CE in the midst of the Medieval epoch, as evaluated for the adjusted calibration R^2 , the validation R^2 , the reduction of error (RE), and the coefficient of efficiency (CE). Available tree-ring sites at 1000 CE are indicated by black circles.

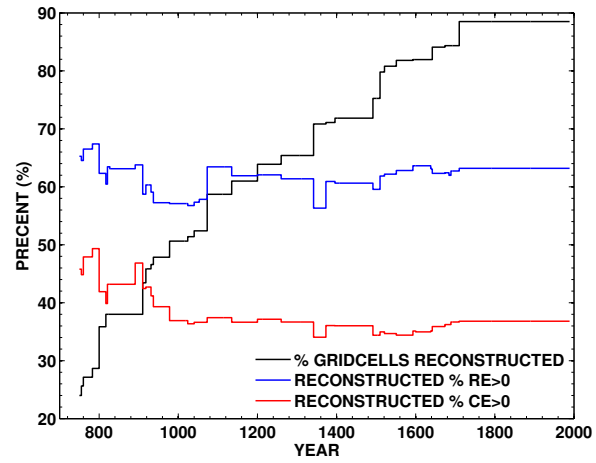


Figure 11: Aggregate temporal reconstruction skill. The percent of all target grid points that are able to be reconstructed for a given year is shown by the black line. For those grid points with a reconstructed value in a given year, the red and blue lines show the percent of those grid points with RE and CE greater than zero.

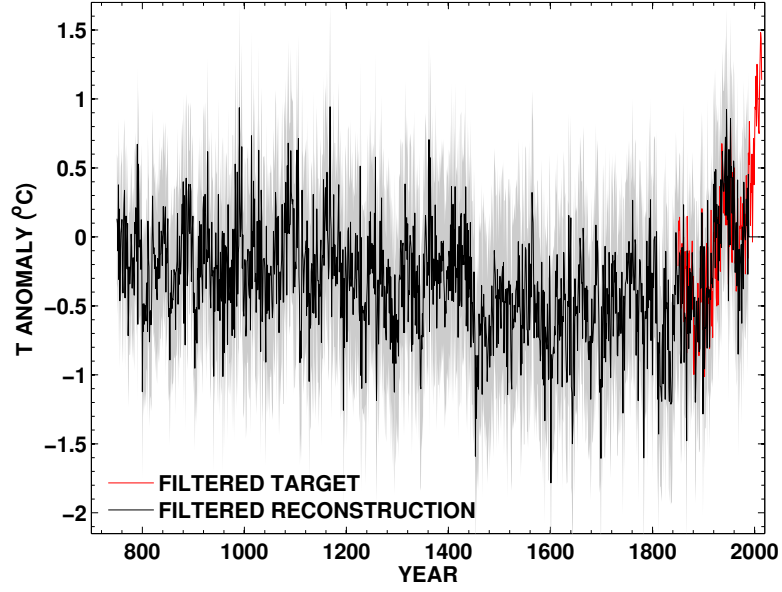


Figure 12: Filtered latitude-weighted mean hemisphere MJJA temperature anomaly reconstruction and target MJJA observational time series. Spatial mean values for both the reconstruction (black) and target (red) MJJA fields are calculated from the set of all grid points that have reconstructed values back to at least 1000 CE and which have an RE score greater than zero at 1000 CE ($n = 229$) and are weighted by latitude. Uncertainty in the reconstruction is indicated by the gray shading, and is calculated as the mean latitude-weighted local mean squared error of validation. The reconstruction and target MJJA temperature series are significantly correlated over their common interval (1850–1988, $n = 139$, $r = 0.78$, $p < 0.001$).

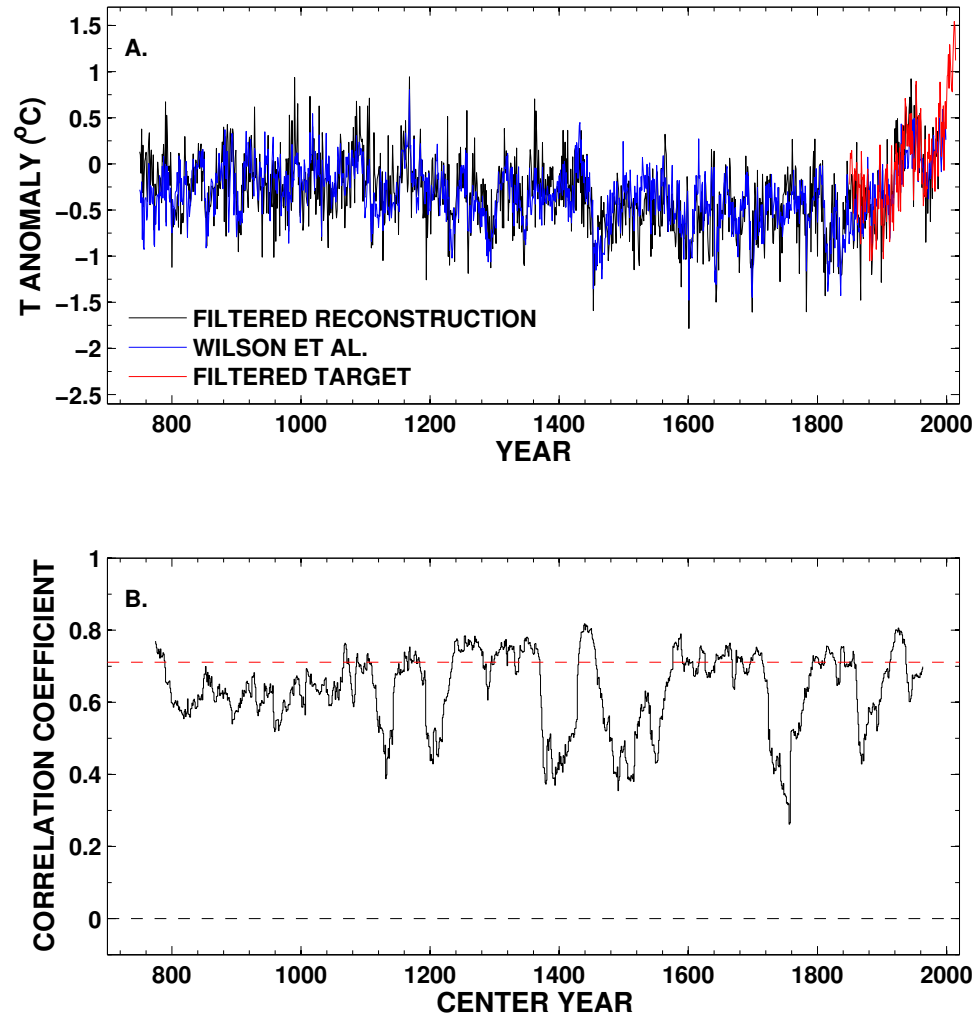


Figure 13: Comparison between time series reconstruction from (blue; Wilson et al., 2016) and the filtered weighted global mean MJJA temperature reconstructed here (black). Time series are shown in (A), and a running correlation (50 year window, 1 year increment) is plotted in (B). The full overall correlation between the two series (750 to 1988 CE, $r = 0.71$) is indicated by the dashed red line in (B).

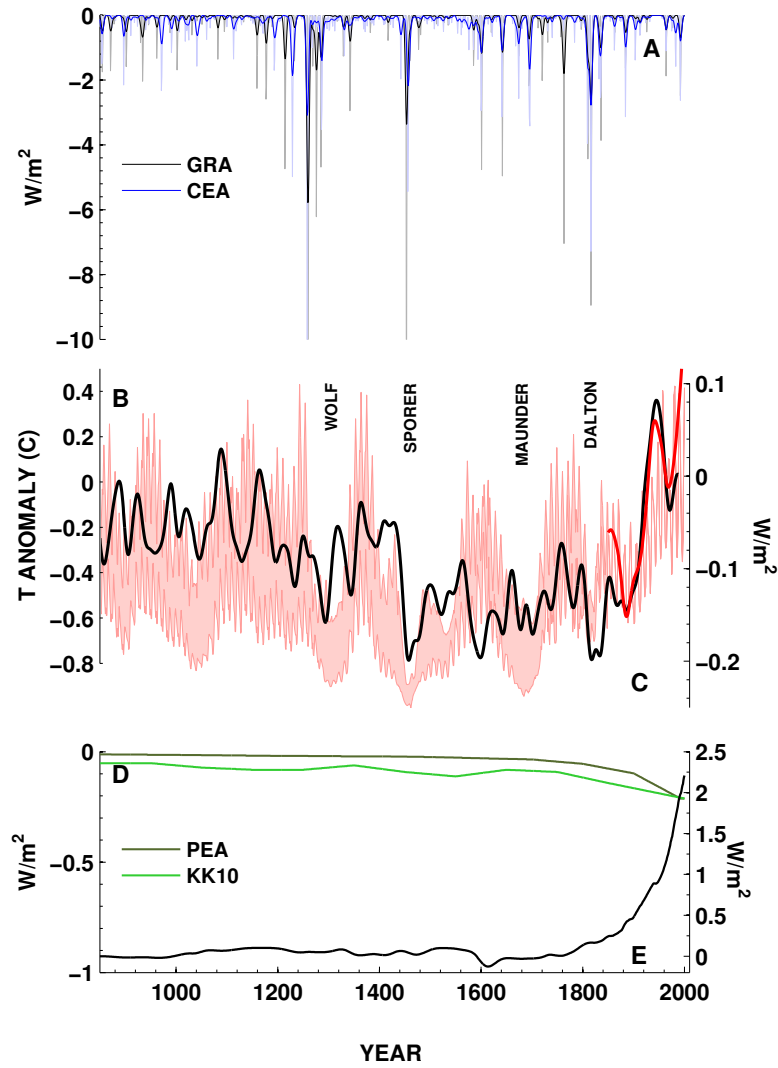


Figure 14: Radiative forcing and reconstructed Northern Hemisphere warm-season temperatures from this study during the last millennium. All forcing series are those compiled by Schmidt et al. (2012) for PMIP3 simulations of the last millennium (version 1.1). (A) Volcanic forcing following Gao et al. (2008) (black/grey, GRA) and Crowley et al. (2008) (blue/light blue, CEA), with individual years as lighter lines and 30-year Gaussian smoothed values in heavy lines. Note that the magnitude of some individual events exceeds the y-axis limits. (B) Northern Hemisphere mean MJJA temperature anomaly time series as described in the text (black line) and corresponding observed temperatures for the same grid points (red line). Here both reconstructed and observed values have been smoothed with a 30 year Gaussian filter. (C) Solar forcing relative to the period 1976 to 2006 CE, with the pink shaded region showing the range of the forcing reconstructions compiled by Schmidt et al. (2012) including Delaygue and Bard (2011), Muscheler et al. (2007), Steinhilber et al. (2009) and Vieira and Solanki (2010). Major solar minima are labeled. (D) Forcing due to land use change from Kaplan et al. (2011) (KK10) and Pongratz et al. (2008) (PEA). (E) Well-mixed greenhouse gas forcing.

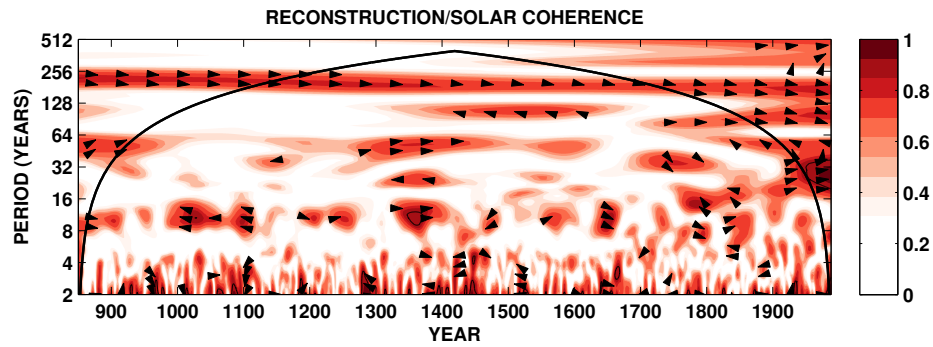


Figure 15: Wavelet coherence (Torrence and Compo, 1998; Grinsted et al., 2004) between our Northern Hemisphere mean MJJA temperature anomaly time series and solar forcing variability from Vieira and Solanki (2010). Arrows indicate the phase of the relationship and for clarity are plotted only where coherence exceeds 0.65. In-phase signals point directly to the right of the plot. Values above the cone of influence (COI; black curve) are potentially influenced by edge effects at that time period and scale.

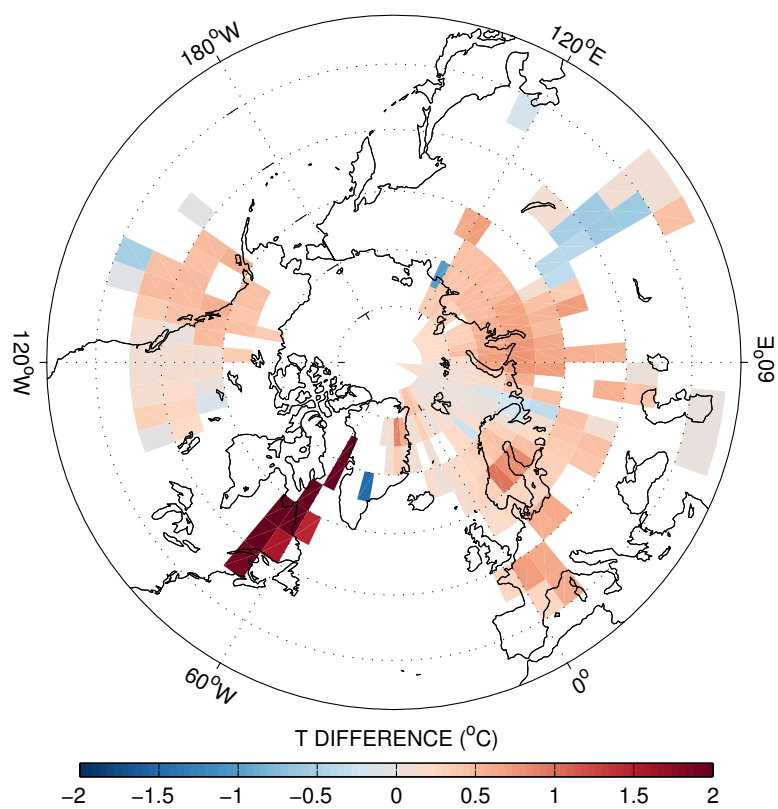


Figure 16: Medieval Climate Anomaly (MCA; 950-1250 CE) vs Little Ice Age (LIA; 1450-1850 CE) mean temperature anomaly fields (MCA-LIA). Only grid points with values reconstructed at $RE > 0$ at 1000 CE are shown.

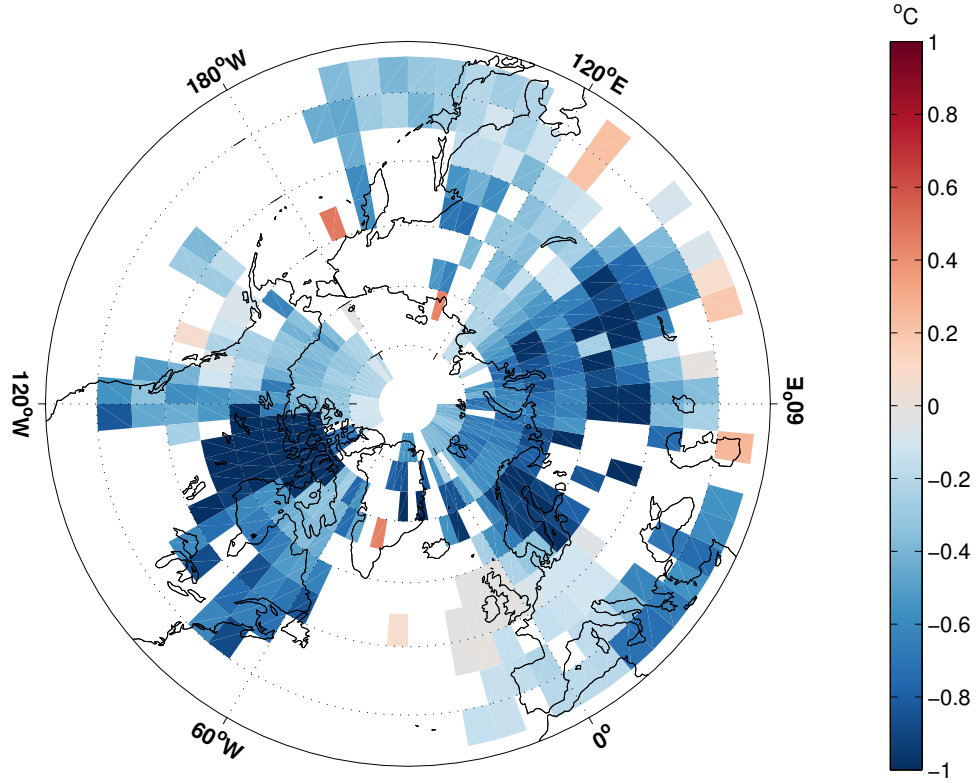


Figure 17: Composite mean reconstructed temperatures following major tropical volcanic eruptions (from Sigl et al. (2015)). Eruption years in the composite ($n = 20$) are those with a global forcing magnitude equal to or larger than that associated with Krakatoa (1884), and include 916, 1108, 1171, 1191, 1230, 1258, 1276, 1286, 1345, 1453, 1458, 1595, 1601, 1641, 1695, 1809, 1815, 1832, 1836, and 1884 CE. Event anomalies are calculated by first subtracting the global field mean over the 3 years prior to the eruption. Only grid points with $RE > 0$ in an event year are averaged to form the composite and only those grid points with values for at least 6 eruptions are plotted.

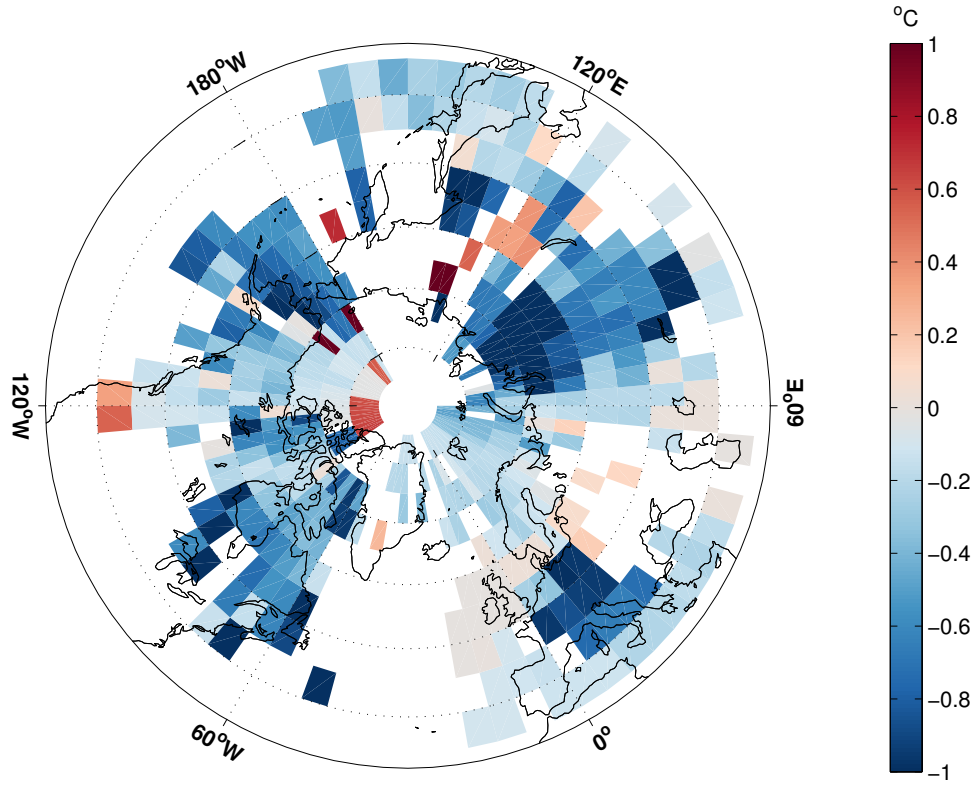


Figure 18: Composite mean reconstructed temperatures following major Northern Hemisphere high latitude volcanic eruptions (from Sigl et al. (2015)). Eruption years in the composite ($n = 5$) are those Northern Hemisphere eruption with a global forcing equal to or larger than the magnitude associated with Katmai (1912), and include 939, 1182 1210, 1783, and 1912 CE. Event anomalies are calculated by first subtracting the global field mean over the 3 years prior to the eruption. Only grid points with $RE > 0$ in an event year are averaged to form the composite and only those grid points with values for at least 2 eruptions are plotted.

788 Ammann, C.M., Joos, F., Schimel, D.S., Otto-Bliesner, B.L., Tomas, R.A.,
789 2007. Solar influence on climate during the past millennium: Results from
790 transient simulations with the NCAR Climate System Model. *Proc. U. S.*
791 *Natl. Acad. Sci.* 104, 3713–3718.

792 Ammann, C.M., Naveau, P., 2003. Statistical analysis of tropical explosive
793 volcanism occurrences over the last 6 centuries. *Geophys. Res. Lett.* 30, 1210.
794 doi:10.1029/2002GL016388.

795 Anchukaitis, K., McKay, N., 2014. PAGES2k: Advances in Climate Field Re-
796 constructions. *PAGES Magazine* 22, 98.

797 Anchukaitis, K.J., Breitenmoser, P., Briffa, K.R., Buchwal, A., Büntgen, U.,
798 Cook, E.R., D’Arrigo, R.D., Esper, J., Evans, M.N., Frank, D., Grudd, H.,
799 Gunnarson, B., Hughes, M.K., Kirdyanov, A.V., Körner, C., Krusic, P.J.,
800 Luckman, B., Melvin, T.M., Salzer, M.W., Shashkin, A.V., Timmreck, C.,
801 Vaganov, E.A., Wilson, R.J., 2012. Tree rings and volcanic cooling. *Nature*
802 *Geosci* 5, 836–837. doi:10.1038/ngeo1645.

803 Anchukaitis, K.J., Buckley, B.M., Cook, E.R., Cook, B.I., D’Arrigo, R., Am-
804 mann, C.M., 2010. The influence of volcanic eruptions on the climate of the
805 Asian monsoon region. *Geophys. Res. Lett.* 37. doi:10.1029/2010GL044843.

806 Anchukaitis, K.J., D’Arrigo, R.D., Andreu-Hayles, L., Frank, D., Verstege,
807 A., Curtis, A., Buckley, B.M., Jacoby, G.C., Cook, E.R., 2013. Tree-
808 Ring-Reconstructed Summer Temperatures from Northwestern North Amer-
809 ica during the Last Nine Centuries. *Journal of Climate* 26, 3001–3012.
810 doi:10.1175/JCLI-D-11-00139.1.

811 Anchukaitis, K.J., Evans, M.N., Kaplan, A., Vaganov, E.A., Hughes, M.K.,
812 Grissino-Mayer, H.D., Cane, M.A., 2006. Forward modeling of regional scale
813 tree-ring patterns in the southeastern United States and the recent influence
814 of summer drought. *Geophys. Res. Lett.* 33. doi:10.1029/2005GL025050.

- 815 Andreu-Hayles, L., D'Arrigo, R.D., Anchukaitis, K.J., Beck, P., Frank, D., Ver-
816 stege, A., Goetz, S., 2011. Varying boreal forest response to Arctic environ-
817 mental change at the Firth River, Alaska. *Environmental Research Letters* 6,
818 045503. doi:10.1088/1748-9326/6/4/045503.
- 819 Andronova, N.G., Schlesinger, M.E., 2000. Causes of global temperature changes
820 during the 19th and 20th centuries. *Geophysical Research Letters* 27, 2137–
821 2140.
- 822 Autin, J., Gennaretti, F., Arseneault, D., Bégin, Y., 2015. Biases in RCS tree
823 ring chronologies due to sampling heights of trees. *Dendrochronologia* 36,
824 13–22.
- 825 Biondi, F., Perkins, D.L., Cayan, D.R., Hughes, M.K., 1999. July temperature
826 during the second millennium reconstructed from Idaho tree rings. *Geophys.*
827 *Res. Lett.* 26, 1445–1448.
- 828 Björklund, J., Gunnarson, B.E., Seftigen, K., Zhang, P., Linderholm, H.W.,
829 2015. Using adjusted Blue Intensity data to attain high-quality summer tem-
830 perature information: A case study from Central Scandinavia. *The Holocene*
831 25, 547–556.
- 832 Björklund, J.A., Gunnarson, B.E., Seftigen, K., Esper, J., Linderholm, H.W.,
833 2014. Blue intensity and density from northern Fennoscandian tree rings, ex-
834 ploring the potential to improve summer temperature reconstructions with
835 earlywood information. *Climate of the Past* 10, 877–885. doi:10.5194/
836 cp-10-877-2014.
- 837 Bowman, A.W., Azzalini, A., 1997. *Applied smoothing techniques for data*
838 *analysis*. Oxford University Press.
- 839 Bradley, R.S., Briffa, K.R., Crowley, T.J., Hughes, M.K., Jones, P.D., Mann,
840 M.E., 2001. The scope of medieval warming. *Science* 292, 2011–2012.

- 841 Breitenmoser, P., Beer, J., Brönnimann, S., Frank, D., Steinhilber, F., Wanner,
842 H., 2012. Solar and volcanic fingerprints in tree-ring chronologies over the
843 past 2000 years. *Palaeogeogr. Palaeoclim. Palaeoecol.* 313–314, 127–139.
- 844 Briffa, K., Jones, P., 1993. Global surface air temperature variations during the
845 twentieth century: Part 2, implications for large-scale high-frequency palaeo-
846 climatic studies. *The Holocene* 3, 77–88.
- 847 Briffa, K.R., 1994. Grasping at shadows? a selective review of the search
848 for sunspot-related variability in tree rings, in: *The Solar Engine and Its*
849 *Influence on Terrestrial Atmosphere and Climate*. Springer Nature, pp. 417–
850 435. doi:10.1007/978-3-642-79257-1_26.
- 851 Briffa, K.R., 1995. Interpreting high-resolution proxy climate data – the example
852 of dendroclimatology, in: von Storch, H., Navarra, A. (Eds.), *Analysis of*
853 *Climate Variability: Applications of Statistical Techniques*. Springer, pp. 77–
854 94. doi:10.1007/978-3-662-03167-4_5.
- 855 Briffa, K.R., 2000. Annual climate variability in the Holocene: interpreting the
856 message of ancient trees. *Quat. Sci. Rev.* 19, 87–105.
- 857 Briffa, K.R., Jones, P.D., Schweingruber, F.H., Karlén, W., Shiyatov, S.G.,
858 1996. Tree-ring variables as proxy-climate indicators: Problems with low-
859 frequency signals, in: *Climatic Variations and Forcing Mechanisms of the*
860 *Last 2000 Years*. Springer Nature, pp. 9–41. URL: [https://doi.org/10.](https://doi.org/10.1007/978-3-642-61113-1_2)
861 [1007/978-3-642-61113-1_2](https://doi.org/10.1007/978-3-642-61113-1_2), doi:10.1007/978-3-642-61113-1_2.
- 862 Briffa, K.R., Jones, P.D., Schweingruber, F.H., Osborn, T.J., 1998a. Influence
863 of volcanic eruptions on Northern Hemisphere summer temperature over the
864 past 600 years. *Nature* 393, 450–455.
- 865 Briffa, K.R., Melvin, T.M., 2011. A closer look at regional curve standardization
866 of tree-ring records: Justification of the need, a warning of some pitfalls, and
867 suggested improvements in its application, in: Hughes, M.K., Diaz, H.F.,
868 Swetnam, T.W. (Eds.), *Dendroclimatology: Progress and Prospects*. Springer

Verlag, volume 11 of *Developments in Paleoenvironmental Research*, pp. 113–
146.

Briffa, K.R., Melvin, T.M., Osborn, T.J., Hantemirov, R.M., Kirdyanov, A.V.,
Mazepa, V.S., Shiyatov, S.G., Esper, J., 2013. Reassessing the evidence
for tree-growth and inferred temperature change during the Common Era
in Yamalia, northwest Siberia. *Quaternary Science Reviews* 72, 83–107.
doi:10.1016/j.quascirev.2013.04.008.

Briffa, K.R., Osborn, T.J., Schweingruber, F.H., 2004. Large-scale temperature
inferences from tree rings: a review. *Global Planetary Change* 40, 11–26.

Briffa, K.R., Osborn, T.J., Schweingruber, F.H., Jones, P.D., Shiyatov, S.G.,
Vaganov, E.A., 2002. Tree-ring width and density data around the Northern
Hemisphere: Part 1, local and regional climate signals. *Holocene* 12, 737–757.

Briffa, K.R., Schweingruber, F.H., Jones, P.D., Osborn, T.J., Harris, I.C., Shiy-
atov, S.G., Vaganov, E.A., Grudd, H., 1998b. Trees tell of past climates: but
are they speaking less clearly today? *Philosophical Transactions of The Royal
Society of London Series B-Biological Sciences* 353, 65–73.

Brohan, P., Allan, R., Freeman, E., Wheeler, D., Wilkinson, C., Williamson,
F., 2012. Constraining the temperature history of the past millennium using
early instrumental observations. *Climate of the Past* 8, 1551–1563. doi:10.
5194/cp-8-1551-2012.

Buckley, B., Anchukaitis, K., Penny, D., Fletcher, R., Cook, E., Sano, M., Nam,
L., Wichienkeo, A., Minh, T., Hong, T., 2010. Climate as a contributing fac-
tor in the demise of Angkor, Cambodia. *Proceedings of the National Academy
of Sciences* 107, 6748–6752.

Büntgen, U., Frank, D.C., Nievergelt, D., Esper, J., 2006. Summer Temperature
Variations in the European Alps, A.D. 755–2004. *Journal of Climate* 19,
5606–5623. doi:10.1175/jcli3917.1.

896 Büntgen, U., Kyncl, T., Ginzler, C., Jacks, D.S., Esper, J., Tegel, W., Heussner,
897 K.U., Kyncl, J., 2013. Filling the Eastern European gap in millennium-
898 long temperature reconstructions. *Proceedings of the National Academy of*
899 *Sciences* 110, 1773–1778. doi:10.1073/pnas.1211485110.

900 Büntgen, U., Myglan, V.S., Ljungqvist, F.C., McCormick, M., Cosmo, N.D.,
901 Sigl, M., Jungclaus, J., Wagner, S., Krusic, P.J., Esper, J., Kaplan, J.O.,
902 de Vaan, M.A.C., Luterbacher, J., Wacker, L., Tegel, W., Kirdyanov, A.V.,
903 2016. Cooling and societal change during the Late Antique Little Ice Age from
904 536 to around 660 AD. *Nature Geoscience* 9, 231–236. doi:10.1038/ngeo2652.

905 Büntgen, U., Tegel, W., Nicolussi, K., McCormick, M., Frank, D., Trouet, V.,
906 Kaplan, J., Herzig, F., Heussner, K., Wanner, H., Luterbacher, J., Esper, J.,
907 2011. 2500 years of European climate variability and human susceptibility.
908 *Science* 331, 578–582.

909 Büntgen, U., Wacker, L., Nicolussi, K., Sigl, M., Gütler, D., Tegel, W., Krusic,
910 P.J., Esper, J., 2014. Extraterrestrial confirmation of tree-ring dating. *Nature*
911 *Climate Change* 4, 404–405.

912 Campbell, R., McCarroll, D., Loader, N.J., Grudd, H., Robertson, I., Jalkanen,
913 R., 2007. Blue intensity in *Pinus sylvestris* tree-rings: developing a new
914 palaeoclimate proxy. *The Holocene* 17, 821–828.

915 Cole-Dai, J., Ferris, D.G., Lanciki, A.L., Savarino, J., Thiemens, M.H., Mc-
916 Connell, J.R., 2013. Two likely stratospheric volcanic eruptions in the 1450s
917 C.E. found in a bipolar, subannually dated 800 year ice core record. *Journal*
918 *of Geophysical Research: Atmospheres* 118, 7459–7466. doi:10.1002/jgrd.
919 50587.

920 Cook, E., Kairiūkštis, L. (Eds.), 1990. *Methods of dendrochronology: applica-*
921 *tions in the environmental sciences.* Kluwer Academic, Dordrecht.

922 Cook, E.R., 1987. The decomposition of tree-ring series for environmental stud-
923 ies. *Tree-Ring Bulletin* 47, 37–59.

924 Cook, E.R., Anchukaitis, K.J., Buckley, B.M., D'Arrigo, R.D., Jacoby, G.C.,
925 Wright, W.E., 2010a. Asian Monsoon Failure and Megadrought During the
926 Last Millennium. *Science* 328, 486–489. doi:10.1126/science.1185188.

927 Cook, E.R., Briffa, K.R., Jones, P.D., 1994. Spatial regression methods in
928 dendroclimatology – a review and comparison of 2 techniques. *Int. J. Climatol.*
929 14, 379–402.

930 Cook, E.R., Briffa, K.R., Meko, D.M., Graybill, D.A., Funkhouser, G., 1995.
931 The Segment Length Curse in long tree-ring chronology development for pa-
932 leoclimatic studies. *Holocene* 5, 229–237.

933 Cook, E.R., Krusic, P.J., Anchukaitis, K.J., Buckley, B.M., Nakatsuka, T., Sano,
934 M., 2013. Tree-ring reconstructed summer temperature anomalies for tem-
935 perate East Asia since 800 CE. *Clim. Dynam.* 41, 2957–2972.

936 Cook, E.R., Meko, D.M., Stahle, D.W., Cleaveland, M.K., 1999. Drought re-
937 constructions for the continental United States. *J. Climate* 12, 1145–1162.

938 Cook, E.R., Seager, R., Heim, R.R., Vose, R.S., Herweijer, C., Woodhouse,
939 C.A., 2010b. Megadroughts in North America: Placing IPCC projections of
940 hydroclimatic change in a long-term paleoclimate context. *Journal of Qua-*
941 *ternary Science* 25, 48–61.

942 Cowtan, K., Way, R.G., 2014. Coverage bias in the HadCRUT4 temperature
943 series and its impact on recent temperature trends. *Quarterly Journal of the*
944 *Royal Meteorological Society* 140, 1935–1944. doi:10.1002/qj.2297.

945 Crowley, T.J., 2000. Causes of climate change over the past 1000 years. *Science*
946 289, 270–277.

947 Crowley, T.J., Zielinski, G., Vinther, B., Udisti, R., Kreutz, K., Cole-Dai, J.,
948 Castellano, E., 2008. Volcanism and the Little Ice Age. *PAGES News* 16,
949 22–23.

950 D'Arrigo, R., Anchukaitis, K.J., Buckley, B., Cook, E.R., Wilson, R., 2011.
951 Regional climatic and North Atlantic Oscillation signatures in West Virginia
952 red cedar over the past millennium. *Global and Planetary Change* 84–85,
953 8–13. doi:10.1016/j.gloplacha.2011.07.003.

954 D'Arrigo, R., Buckley, B., Kaplan, S., Woollett, J., 2003. Interannual to multi-
955 decadal modes of Labrador climate variability inferred from tree rings. *Clim.*
956 *Dynam.* 20, 219–228.

957 D'Arrigo, R., Jacoby, G., Free, R., 1992. Tree-ring width and maximum late-
958 wood density at the North American tree line: parameters of climatic change.
959 *Canadian Journal of Forest Research* 22, 1290–1296.

960 D'Arrigo, R., Mashig, E., Frank, D., Jacoby, G., Wilson, R., 2004. Recon-
961 structed warm season temperatures for Nome, Seward Peninsula, Alaska.
962 *Geophys. Res. Lett.* 31. doi:10.1029/2004g1019756.

963 D'Arrigo, R., Wilson, R., Anchukaitis, K.J., 2013. Volcanic cooling signal in tree
964 ring temperature records for the past millennium. *J. Geophys. Res. Atmos.*
965 118, 9000–9010. doi:10.1002/jgrd.50692.

966 D'Arrigo, R., Wilson, R., Liepert, B., Cherubini, P., 2008. On the ‘Divergence
967 Problem’ in Northern Forests: A review of the tree-ring evidence and pos-
968 sible causes. *Global and Planetary Change* 60, 289–305. doi:10.1016/j.
969 gloplacha.2007.03.004.

970 D'Arrigo, R., Wilson, R., Wiles, G., Anchukaitis, K., Solomina, O., Davi, N.,
971 Deser, C., Dolgova, E., 2015. Tree-ring reconstructed temperature index for
972 coastal northern Japan: implications for western North Pacific variability.
973 *International Journal of Climatology* 35, 3713–3720.

974 D'Arrigo, R.D., Jacoby, G.C., Buckley, B.M., Sakulich, J., Frank, D., Wilson,
975 R., Curtis, A., Anchukaitis, K.J., 2009. Tree growth and inferred tempera-
976 ture variability at the North American Arctic treeline. *Global and Planetary*
977 *Change* 65, 71–82.

978 D'Arrigo, R.D., Wilson, R., Jacoby, G.C., 2006. On the long-term context
979 for late twentieth century warming. *J. Geophys. Res.* 111. doi:10.1029/
980 2005JD006352.

981 Davi, N., D'Arrigo, R., Jacoby, G., Cook, E., Anchukaitis, K., Nachin, B., Rao,
982 M., Leland, C., 2015. A long-term context (931–2005 C.E.) for rapid warming
983 over Central Asia. *Quaternary Science Reviews* 121, 89–97. doi:10.1016/j.
984 quascirev.2015.05.020.

985 Davi, N.K., Jacoby, G.C., Wiles, G.C., 2003. Boreal temperature variability
986 inferred from maximum latewood density and tree-ring width data, Wrangell
987 Mountain region, alaska. *Quat. Res.* 60, 252–262.

988 Delaygue, G., Bard, E., 2011. An Antarctic view of Beryllium-10 and solar
989 activity for the past millennium. *Clim. Dynam.* 36, 2201–2218. doi:10.1007/
990 s00382-010-0795-1.

991 Dorado-Liñán, I., Büntgen, U., González-Rouco, F., Zorita, E., Montávez, J.P.,
992 Gómez-Navarro, J.J., Brunet, M., Heinrich, I., Helle, G., Gutiérrez, E., 2012.
993 Estimating 750 years of temperature variations and uncertainties in the Pyre-
994 nees by tree-ring reconstructions and climate simulations. *Climate of the Past*
995 8, 919–933. doi:10.5194/cp-8-919-2012.

996 Edwards, T.L., Crucifix, M., Harrison, S.P., 2007. Using the past to constrain
997 the future: how the palaeorecord can improve estimates of global warming.
998 *Progress in Physical Geography* 31, 481–500.

999 Emile-Geay, J., Cobb, K.M., Mann, M.E., Wittenberg, A.T., 2013. Estimating
1000 central equatorial Pacific SST variability over the past millennium. Part II:
1001 reconstructions and implications. *Journal of Climate* 26, 2329–2352.

1002 Esper, J., Büntgen, U., Luterbacher, J., Krusic, P.J., 2013a. Testing the hypoth-
1003 esis of post-volcanic missing rings in temperature sensitive dendrochronolog-
1004 ical data. *Dendrochronologia* 31, 216–222. doi:10.1016/j.dendro.2012.11.
1005 002.

1006 Esper, J., Cook, E.R., Schweingruber, F.H., 2002. Low-frequency signals in long
1007 tree-ring chronologies for reconstructing past temperature variability. *Science*
1008 295, 2250–2253.

1009 Esper, J., D  thorn, E., Krusic, P.J., Timonen, M., B  ntgen, U., 2014.
1010 Northern European summer temperature variations over the Common Era
1011 from integrated tree-ring density records. *J. Quaternary Sci.* 29, 487–494.
1012 doi:10.1002/jqs.2726.

1013 Esper, J., Frank, D., B  ntgen, U., Verstege, A., Hantemirov, R.M., Kirdyanov,
1014 A.V., 2010. Trends and uncertainties in Siberian indicators of 20th century
1015 warming. *Global Change Biol.* 16, 386–398.

1016 Esper, J., Frank, D., B  ntgen, U., Verstege, A., Luterbacher, J., Xoplaki, E.,
1017 2007. Long-term drought severity variations in Morocco. *Geophys. Res. Lett.*
1018 34. doi:10.1029/2007GL030844.

1019 Esper, J., Frank, D.C., Timonen, M., Zorita, E., Wilson, R.J.S., Luterbacher,
1020 J., Holzkamper, S., Fischer, N., Wagner, S., Nievergelt, D., Verstege, A.,
1021 B  ntgen, U., 2012. Orbital forcing of tree-ring data. *Nature Clim. Change* 2,
1022 862–866. doi:10.1038/nclimate1589.

1023 Esper, J., Krusic, P.J., Ljungqvist, F.C., Luterbacher, J., Carrer, M., Cook, E.,
1024 Davi, N.K., Hartl-Meier, C., Kirdyanov, A., Konter, O., et al., 2016. Rank-
1025 ing of tree-ring based temperature reconstructions of the past millennium.
1026 *Quaternary Science Reviews* 145, 134–151.

1027 Esper, J., Schneider, L., Krusic, P.J., Luterbacher, J., B  ntgen, U., Timonen,
1028 M., Sirocko, F., Zorita, E., 2013b. European summer temperature response
1029 to annually dated volcanic eruptions over the past nine centuries. *Bulletin of*
1030 *Volcanology* 75. doi:10.1007/s00445-013-0736-z.

1031 Esper, J., Schneider, L., Smerdon, J.E., Sch  ne, B.R., B  ntgen, U., 2015. Sig-
1032 nals and memory in tree-ring width and density data. *Dendrochronologia* 35,
1033 62–70.

- 1034 Esper, J., Wilson, R.J.S., Frank, D.C., Moberg, A., Wanner, H., Luterbacher,
1035 J., 2005. Climate: past ranges and future changes. *Quat. Sci. Rev.* 24, 2164–
1036 2166.
- 1037 Estrada, F., Perron, P., Martínez-López, B., 2013. Statistically derived contribu-
1038 tions of diverse human influences to twentieth-century temperature changes.
1039 *Nature Geoscience* 6, 1050–1055.
- 1040 Evans, M., Tolwinski-Ward, S., Thompson, D., Anchukaitis, K., 2013. Applica-
1041 tions of proxy system modeling in high resolution paleoclimatology. *Quater-
1042 nary Science Reviews* 76, 16–28. doi:10.1016/j.quascirev.2013.05.024.
- 1043 Evans, M.N., Kaplan, A., Cane, M.A., 2002. Pacific sea surface temperature field
1044 reconstruction from coral $\delta^{18}\text{O}$ data using reduced space objective analysis.
1045 *Paleoceanography* 17. doi:10.1029/2000PA000590.
- 1046 Evans, M.N., Kaplan, A., Cane, M.A., Villalba, R., 2001. Globality and optimal-
1047 ity in climate field reconstructions from proxy data, in: Markgraf, V. (Ed.),
1048 *Interhemispheric Climate Linkages*, Cambridge University Press, Cambridge,
1049 UK. pp. 53–72.
- 1050 Fernández-Donado, L., González-Rouco, J.F., Raible, C.C., Ammann, C.M.,
1051 Barriopedro, D., García-Bustamante, E., Jungclaus, J.H., Lorenz, S.J., Luter-
1052 bacher, J., Phipps, S.J., Servonnat, J., Swingedouw, D., Tett, S.F.B., Wagner,
1053 S., Yiou, P., Zorita, E., 2013. Large-scale temperature response to external
1054 forcing in simulations and reconstructions of the last millennium. *Climate of
1055 the Past* 9, 393–421. doi:10.5194/cp-9-393-2013.
- 1056 Frank, D., Büntgen, U., Böhm, R., Maugeri, M., Esper, J., 2007. Warmer
1057 early instrumental measurements versus colder reconstructed temperatures:
1058 shooting at a moving target. *Quat. Sci. Rev.* 26, 3298–3310.
- 1059 Frank, D., Esper, J., Zorita, E., Wilson, R., 2010. A noodle, hockey stick, and
1060 spaghetti plate: a perspective on high-resolution paleoclimatology. *WIREs
1061 Clim Chg* 1, 507–516. doi:10.1002/wcc.53.

1062 Fritts, H.C., 1976. *Tree Rings and Climate*. Academic Press, New York.

1063 Fritts, H.C., 1991. *Reconstructing large-scale climatic patterns from tree-ring*
1064 *data: A diagnostic analysis*. University of Arizona Press, London.

1065 Gallant, A.J., Phipps, S.J., Karoly, D.J., Mullan, A.B., Lorrey, A.M., 2013.
1066 *Nonstationary Australasian teleconnections and implications for paleoclimate*
1067 *reconstructions*. *Journal of Climate* 26, 8827–8849.

1068 Gao, C., Robock, A., Ammann, C.M., 2008. *Volcanic forcing of climate over*
1069 *the past 1500 years: an improved ice-core-based index for climate models*. *J.*
1070 *Geophys. Res.* 113. doi:10.1029/2008JD010239.

1071 Gao, C.C., Robock, A., Self, S., Witter, J.B., Steffenson, J.P., Clausen, H.B.,
1072 Siggaard-Andersen, M.L., Johnsen, S., Mayewski, P.A., Ammann, C., 2006.
1073 *The 1452 or 1453 AD Kuwae eruption signal derived from multiple ice core*
1074 *records: Greatest volcanic sulfate event of the past 700 years*. *J. Geophys.*
1075 *Res. - Atmospheres* 111. doi:10.1029/2005JD006710.

1076 Gennaretti, F., Arseneault, D., Nicault, A., Perreault, L., Bégin, Y., 2014.
1077 *Volcano-induced regime shifts in millennial tree-ring chronologies from north-*
1078 *eastern North America*. *Proceedings of the National Academy of Sciences* 111,
1079 10077–10082.

1080 Gershunov, A., Barnett, T.P., 1998. *Interdecadal modulation of ENSO telecon-*
1081 *nections*. *Bull. Amer. Meteorol. Soc.* 79, 2715–2725.

1082 Gillett, N.P., Arora, V.K., Flato, G.M., Scinocca, J.F., von Salzen, K., 2012.
1083 *Improved constraints on 21st-century warming derived using 160 years of tem-*
1084 *perature observations*. *Geophys. Res. Lett.* 39. doi:10.1029/2011gl050226.

1085 Goosse, H., 2016. *Reconstructed and simulated temperature asymmetry be-*
1086 *tween continents in both hemispheres over the last centuries*. *Clim Dyn*
1087 doi:10.1007/s00382-016-3154-z.

1088 Grinsted, A., Moore, J.C., Jevrejeva, S., 2004. Application of the cross wavelet
1089 transform and wavelet coherence to geophysical time series. *Nonlinear Pro-*
1090 *cesses in Geophysics* 11, 561–566.

1091 Hakim, G.J., Emile-Geay, J., Steig, E.J., Noone, D., Anderson, D.M., Tardif,
1092 R., Steiger, N., Perkins, W.A., 2016. The last millennium climate reanaly-
1093 sis project: Framework and first results. *Journal of Geophysical Research:*
1094 *Atmospheres* 121, 6745–6764. doi:10.1002/2016jd024751.

1095 Harris, I., Jones, P.D., Osborn, T.J., Lister, D.H., 2013. Updated high-resolution
1096 grids of monthly climatic observations: the CRU TS3.10 Dataset. *Int. J.*
1097 *Climatol.* doi:10.1002/joc.3711.

1098 Harrison, S., Bartlein, P., Izumi, K., Li, G., Annan, J., Hargreaves, J., Bra-
1099 connot, P., Kageyama, M., 2015. Evaluation of CMIP5 palaeo-simulations to
1100 improve climate projections. *Nature Climate Change* 5, 735–743.

1101 Haurwitz, M.W., Brier, G.W., 1981. A critique of the superposed epoch analysis
1102 method- Its application to solar-weather relations. *Monthly Weather Review*
1103 109, 2074–2079.

1104 Hegerl, G., Stott, P., 2014. From past to future warming. *Science* 343, 844–845.

1105 Hegerl, G.C., Crowley, T.J., Allen, M., Hyde, W.T., Pollack, H.N., Smerdon, J.,
1106 Zorita, E., 2007. Detection of human influence on a new, validated 1500-year
1107 temperature reconstruction. *J. Climate* 20, 650–666.

1108 Hegerl, G.C., Crowley, T.J., Baum, S.K., Kim, K.Y., Hyde, W.T., 2003. De-
1109 tection of volcanic, solar and greenhouse gas signals in paleo-reconstructions
1110 of Northern Hemispheric temperature. *Geophys. Res. Lett.* 30. doi:10.1029/
1111 2002GL016635.

1112 Hegerl, G.C., Hasselmann, K., Cubasch, U., Mitchell, J., Roeckner, E., Voss, R.,
1113 Waszkewitz, J., 1997. Multi-fingerprint detection and attribution analysis of
1114 greenhouse gas, greenhouse gas-plus-aerosol and solar forced climate change.
1115 *Climate Dynamics* 13, 613–634.

1116 Hegerl, G.C., Karl, T.R., Allen, M., Bindoff, N.L., Gillett, N., Karoly, D.,
1117 Zhang, X., Zwiers, F., 2006. Climate change detection and attribution:
1118 Beyond mean temperature signals. *Journal of Climate* 19, 5058–5077.
1119 doi:10.1175/jcli3900.1.

1120 Hegerl, G.C., Russon, T., 2011. Using the past to predict the future? *Science*
1121 334, 1360–1361.

1122 Helama, S., Vartiainen, M., Holopainen, J., Mäkelä, H., Kolström, T.,
1123 Meriläinen, J., 2014. A palaeotemperature record for the Finnish Lakeland
1124 based on microdensitometric variations in tree rings. *Geochronometria* 41.
1125 doi:10.2478/s13386-013-0163-0.

1126 Hughes, M., 2002. Dendrochronology in climatology - the state of the art.
1127 *Dendrochronologia* 20, 95–116.

1128 Hughes, M.K., Diaz, H.F., 1994. Was there a ‘medieval warm period’ and if so.
1129 *Clim. Change* 26, 109–142.

1130 Hughes, M.K., Vaganov, E.A., Shiyatov, S., Touchan, R., Funkhouser, G., 1999.
1131 Twentieth-century summer warmth in northern Yakutia in a 600-year context.
1132 *Holocene* 9, 629–634.

1133 Jacoby, G.C., D’Arrigo, R.D., 1995. Tree ring width and density evidence of
1134 climatic and potential forest change in Alaska. *Global Biogeochemical Cycles*
1135 9, 227–234.

1136 Jacoby, G.C., Lovelius, N.V., Shumilov, O.I., Raspopov, O.M., Karbainov, J.M.,
1137 Frank, D.C., 2000. Long-term temperature trends and tree growth in the
1138 Taymir region of northern Siberia. *Quat. Res.* 53, 312–318.

1139 Jones, G.S., Stott, P.A., Christidis, N., 2013. Attribution of observed historical
1140 near-surface temperature variations to anthropogenic and natural causes us-
1141 ing CMIP5 simulations. *Journal of Geophysical Research: Atmospheres* 118,
1142 4001–4024.

1143 Jones, P.D., Briffa, K.R., Osborn, T.J., Lough, J.M., van Ommen, T.D.,
1144 Vinther, B.M., Luterbacher, J., Wahl, E.R., Zwiers, F.W., Mann, M.E.,
1145 Schmidt, G.A., Ammann, C.M., Buckley, B.M., Cobb, K.M., Esper, J.,
1146 Goosse, H., Graham, N., Jansen, E., Kiefer, T., Kull, C., Küttel, M., Mosley-
1147 Thompson, E., Overpeck, J.T., Riedwyl, N., Schulz, M., Tudhope, A.W., Vil-
1148 lalba, R., Wanner, H., Wolff, E., Xoplaki, E., 2009. High-resolution palaeo-
1149 climatology of the last millennium: a review of current status and future
1150 prospects. *The Holocene* 19, 3–49. doi:10.1177/0959683608098952.

1151 Jones, P.D., Lister, D.H., Osborn, T.J., Harpham, C., Salmon, M., Morice, C.P.,
1152 2012. Hemispheric and large-scale land-surface air temperature variations: An
1153 extensive revision and an update to 2010. *Journal of Geophysical Research:*
1154 *Atmospheres* 117. doi:10.1029/2011jd017139.

1155 Jones, P.D., Osborn, T.J., Briffa, K.R., 1997. Estimating sampling errors in
1156 large-scale temperature averages. *J. Climate* 10, 2548–2568.

1157 Jull, A.J.T., Panyushkina, I.P., Lange, T.E., Kukarskih, V.V., Myglan, V.S.,
1158 Clark, K.J., Salzer, M.W., Burr, G.S., Leavitt, S.W., 2014. Excursions in the
1159 14 C record at A.D. 774–775 in tree rings from Russia and America. *Geophys.*
1160 *Res. Lett.* 41, 3004–3010. doi:10.1002/2014gl059874.

1161 Kageyama, M., Braconnot, P., Harrison, S.P., Haywood, A.M., Jungclaus, J.,
1162 Otto-Bliesner, B.L., Peterschmitt, J.Y., Abe-Ouchi, A., Albani, S., Bartlein,
1163 P.J., Brierley, C., Crucifix, M., Dolan, A., Fernandez-Donado, L., Fischer,
1164 H., Hopcroft, P.O., Ivanovic, R.F., Lambert, F., Lunt, D.J., Mahowald, N.M.,
1165 Peltier, W.R., Phipps, S.J., Roche, D.M., Schmidt, G.A., Tarasov, L., Valdes,
1166 P.J., Zhang, Q., Zhou, T., 2016. PMIP4-CMIP6: the contribution of the pa-
1167 leoclimate modelling intercomparison project to CMIP6. *Geoscientific Model*
1168 *Development Discussions* doi:10.5194/gmd-2016-106.

1169 Kaplan, J.O., Krumhardt, K.M., Ellis, E.C., Ruddiman, W.F., Lemmen,
1170 C., Goldewijk, K.K., 2011. Holocene carbon emissions as a result of an-

thropogenic land cover change. *The Holocene* 21, 775–791. doi:10.1177/
0959683610386983.

Kaufman, D., 2014. A community-driven framework for climate reconstructions.
Eos, Transactions American Geophysical Union 95, 361–362.

Keigwin, L.D., Sachs, J.P., Rosenthal, Y., 2003. A 1600-year history of the
Labrador Current off Nova Scotia. *Climate Dynamics* 21, 53–62. doi:10.
1007/s00382-003-0316-6.

Kennedy, J.J., Rayner, N.A., Smith, R.O., Parker, D.E., Saunby, M., 2011a.
Reassessing biases and other uncertainties in sea surface temperature obser-
vations measured in situ since 1850: 1. measurement and sampling uncertain-
ties. *J. Geophys. Res.* 116. doi:10.1029/2010jd015218.

Kennedy, J.J., Rayner, N.A., Smith, R.O., Parker, D.E., Saunby, M., 2011b.
Reassessing biases and other uncertainties in sea surface temperature observa-
tions measured in situ since 1850: 2. biases and homogenization. *J. Geophys.*
Res. 116. doi:10.1029/2010jd015220.

Klesse, S., Ziehmer, M., Rousakis, G., Trouet, V., Frank, D., 2015. Synop-
tic drivers of 400 years of summer temperature and precipitation variabil-
ity on Mt. Olympus, Greece. *Clim. Dynam.* 45, 807–824. doi:10.1007/
s00382-014-2313-3.

Lavigne, F., Degeai, J.P., Komorowski, J.C., Guillet, S., Robert, V., Lahitte,
P., Oppenheimer, C., Stoffel, M., Vidal, C.M., Surono, Pratomo, I., Wassmer,
P., Hajdas, I., Hadmoko, D.S., de Belizal, E., 2013. Source of the great A.D.
1257 mystery eruption unveiled, Samalas volcano, Rinjani Volcanic Complex,
Indonesia. *Proceedings of the National Academy of Sciences* 110, 16742–
16747. doi:10.1073/pnas.1307520110.

Lean, J.L., Rind, D.H., 2008. How natural and anthropogenic influences alter
global and regional surface temperatures: 1889 to 2006. *Geophys. Res. Lett.*
35. doi:10.1029/2008gl034864.

1199 Lee, T.C.K., Zwiers, F.W., Tsao, M., 2008. Evaluation of proxy-based millennial
1200 reconstruction methods. *Climate Dyn.* 31, 263–281.

1201 Lehner, F., Raible, C.C., Stocker, T.F., 2012. Testing the robustness of a pre-
1202 cipitation proxy-based North Atlantic Oscillation reconstruction. *Quaternary*
1203 *Science Reviews* 45, 85–94.

1204 Lewis, S.C., LeGrande, A.N., 2015. Stability of ENSO and its tropical Pacific
1205 teleconnections over the Last Millennium. *Climate of the Past* 11, 1347–1360.
1206 doi:10.5194/cp-11-1347-2015.

1207 Li, B., Nychka, D., Ammann, C., 2010. The value of multiproxy reconstruction
1208 of past climate. *J. Am. Stat. Assoc.* 105, 883–895.

1209 Linderholm, H.W., Björklund, J., Seftigen, K., Gunnarson, B.E., Fuentes, M.,
1210 2015. Fennoscandia revisited: a spatially improved tree-ring reconstruction
1211 of summer temperatures for the last 900 years. *Clim. Dynam.* 45, 933–947.
1212 doi:10.1007/s00382-014-2328-9.

1213 Luckman, B.H., Wilson, R.J.S., 2005. Summer temperatures in the Canadian
1214 Rockies during the last millennium: a revised record. *Clim. Dynam.* 24, 131–
1215 144.

1216 Ludlow, F., Stine, A.R., Leahy, P., Murphy, E., Mayewski, P.A., Taylor, D.,
1217 Killen, J., Baillie, M.G., Hennessy, M., Kiely, G., 2013. Medieval Irish chron-
1218 icles reveal persistent volcanic forcing of severe winter cold events, 431–1649
1219 CE. *Environmental Research Letters* 8, 024035. doi:10.1088/1748-9326/8/
1220 2/024035.

1221 Mann, M.E., Bradley, R.S., Hughes, M.K., 1998. Global-scale temperature
1222 patterns and climate forcing over the past six centuries. *Nature* 392, 779–787.

1223 Mann, M.E., Fuentes, J.D., Rutherford, S., 2012. Underestimation of volcanic
1224 cooling in tree-ring-based reconstructions of hemispheric temperatures. *Nature*
1225 *Geoscience* 5, 202–205.

1226 Mann, M.E., Rutherford, S., 2002. Climate reconstruction using 'pseudoproxies'.
1227 Geophys. Res. Lett. 29. doi:10.1029/2001GL014554.

1228 Mann, M.E., Rutherford, S., Schurer, A., Tett, S.F., Fuentes, J.D., 2013. Dis-
1229 crepancies between the modeled and proxy-reconstructed response to vol-
1230 canic forcing over the past millennium: Implications and possible mechanisms.
1231 Journal of Geophysical Research: Atmospheres 118, 7617–7627.

1232 Mann, M.E., Rutherford, S., Wahl, E., Ammann, C., 2005. Testing the fidelity
1233 of methods used in proxy-based reconstructions of past climate. J. Climate
1234 18, 4097–4107.

1235 Mann, M.E., Rutherford, S., Wahl, E., Ammann, C., 2007. Robustness of proxy-
1236 based climate field reconstruction methods. J. Geophys. Res. 112. doi:10.
1237 1029/2006JD008272, 2007.

1238 Mann, M.E., Zhang, Z., Hughes, M.K., Bradley, R.S., Miller, S.K., Rutherford,
1239 S., Ni, F., 2008. Proxy-based reconstructions of hemispheric and global surface
1240 temperature variations over the past two millennia. Proc. Natl. Acad. Sci.
1241 USA 105, 13252–13257.

1242 Mann, M.E., Zhang, Z., Rutherford, S., Bradley, R.S., Hughes, M.K., Shindell,
1243 D., Ammann, C., Faluvegi, G., Ni, F., 2009. Global signatures and dynamical
1244 origins of the Little Ice Age and Medieval Climate Anomaly. Science 326,
1245 1256–1260.

1246 Masson-Delmotte, V., Schulz, M., Abe-Ouchi, A., Beer, J., Ganopolski, A.,
1247 González Rouco, J., Jansen, E., Lambeck, K., Luterbacher, J., Naish, T.,
1248 Osborn, T., Otto-Bliesner, B., Quinn, T., Ramesh, R., Rojas, M., Shao, X.,
1249 Timmermann, A., 2013. Information from paleoclimate archives, in: Stocker,
1250 T., Qin, D., Plattner, G.K., Tignor, M., Allen, S., Boschung, J., Nauels, A.,
1251 Xia, Y., Bex, V., Midgley, P. (Eds.), Climate Change 2013: The Physical Sci-
1252 ence Basis. Contribution of Working Group I to the Fifth Assessment Report
1253 of the Intergovernmental Panel on Climate Change, Cambridge University

1254 Press, Cambridge, United Kingdom and New York, NY, USA. pp. 383–464.
1255 doi:10.1017/CB09781107415324.013.

1256 Matskovsky, V., Helama, S., 2016. Direct transformation of tree-ring measure-
1257 ments into palaeoclimate reconstructions in three-dimensional space. *The*
1258 *Holocene* 26, 439–449.

1259 Matskovsky, V.V., Helama, S., 2014. Testing long-term summer temperature
1260 reconstruction based on maximum density chronologies obtained by reanalysis
1261 of tree-ring data sets from northernmost Sweden and Finland. *Climate of the*
1262 *Past* 10, 1473–1487. doi:10.5194/cp-10-1473-2014.

1263 Matthews, J.A., Briffa, K.R., 2005. The ‘Little Ice Age’: Re-evaluation of an
1264 evolving concept. *Geografiska Annaler Series A – Physical Geography* 87A,
1265 17–36.

1266 McCarroll, D., Loader, N.J., Jalkanen, R., Gagen, M.H., Grudd, H., Gun-
1267 nerson, B.E., Kirchhefer, A.J., Friedrich, M., Linderholm, H.W., Lindholm,
1268 M., Boettger, T., Los, S.O., Remmele, S., Kononov, Y.M., Yamazaki, Y.H.,
1269 Young, G.H., Zorita, E., 2013. A 1200-year multiproxy record of tree growth
1270 and summer temperature at the northern pine forest limit of Europe. *The*
1271 *Holocene* 23, 471–484. doi:10.1177/0959683612467483.

1272 McCarroll, D., Pettigrew, E., Luckman, A., Guibal, F., Edouard, J.L., 2002.
1273 Blue Reflectance Provides a Surrogate for Latewood Density of High-Latitude
1274 Pine Tree Rings. *Arctic, Antarctic, and Alpine Research* 34, 450–453. doi:10.
1275 2307/1552203.

1276 McCormick, M., Dutton, P.E., Mayewski, P.A., 2007. Volcanoes and the climate
1277 forcing of Carolingian Europe, AD 750–950. *Speculum* 82, 865–895.

1278 McGregor, H.V., Evans, M.N., Goosse, H., Leduc, G., Martrat, B., Addison,
1279 J.A., Mortyn, P.G., Oppo, D.W., Seidenkrantz, M.S., Sicre, M.A., Phipps,
1280 S.J., Selvaraj, K., Thirumalai, K., Filipsson, H.L., Ersek, V., 2015. Robust

1281 global ocean cooling trend for the pre-industrial common era. *Nature Geo-*
1282 *science* 8, 671–677. doi:10.1038/ngeo2510.

1283 McKay, N.P., Kaufman, D.S., 2014. An extended Arctic proxy temperature
1284 database for the past 2,000 years. *Scientific Data* 1. doi:10.1038/sdata.
1285 2014.26.

1286 Meehl, G.A., Washington, W.M., Ammann, C.M., Arblaster, J.M., Wigley,
1287 T.M.L., Tebaldi, C., 2004. Combinations of natural and anthropogenic forc-
1288 ings in twentieth-century climate. *J. Climate* 17, 3721–3727.

1289 Meko, D., 1997. Dendroclimatic reconstruction with time varying predictor
1290 subsets of tree indices. *J. Climate* 10, 687–696.

1291 Melvin, T., Briffa, K., 2008. A ‘signal-free’ approach to dendroclimatic stan-
1292 dardisation. *Dendrochronologia* 26, 71–86.

1293 Melvin, T.M., 2004. Historical growth rates and changing climatic sensitivity
1294 of boreal conifers. Ph.D. thesis. University of East Anglia. Norwich, United
1295 Kingdom.

1296 Michaelson, J., 1987. Cross-validation in statistical climate forecast models. *J.*
1297 *Climate Appl. Meteor.* 26, 1589–1600.

1298 Morice, C.P., Kennedy, J.J., Rayner, N.A., Jones, P.D., 2012. Quantifying
1299 uncertainties in global and regional temperature change using an ensemble
1300 of observational estimates: The HadCRUT4 data set. *J. Geophys. Res.* 117.
1301 doi:10.1029/2011JD017187.

1302 Muscheler, R., Joos, F., Beer, J., Müller, S.A., Vonmoos, M., Snowball, I., 2007.
1303 Solar activity during the last 1000yr inferred from radionuclide records. *Quat.*
1304 *Sci. Rev.* 26, 82–97. doi:10.1016/j.quascirev.2006.07.012.

1305 Naulier, M., Savard, M.M., Bégin, C., Gennaretti, F., Arseneault, D., Marion,
1306 J., Nicault, A., Bégin, Y., 2015. A millennial summer temperature recon-
1307 struction for northeastern Canada using oxygen isotopes in subfossil trees.
1308 *Climate of the Past* 11, 1153–1164. doi:10.5194/cp-11-1153-2015.

1309 Ogurtsov, M., Veretenenko, S., Lindholm, M., Jalkanen, R., 2016. Possible solar-
1310 climate imprint in temperature proxies from the middle and high latitudes of
1311 North America. *Advances in Space Research* 57, 1112–1117. doi:10.1016/j.
1312 **asr**.2015.12.026.

1313 Oman, L., Robock, A., Stenchikov, G., Schmidt, G.A., Ruedy, R., 2005. Cli-
1314 matic response to high-latitude volcanic eruptions. *J. Geophys. Res.* 110.
1315 doi:10.1029/2004JD005487.

1316 Ortega, P., Lehner, F., Swingedouw, D., Masson-Delmotte, V., Raible, C.C.,
1317 Casado, M., Yiou, P., 2015. A model-tested North Atlantic Oscillation re-
1318 construction for the past millennium. *Nature* 523, 71–74. doi:10.1038/
1319 **nature14518**.

1320 PAGES 2k-PMIP3 group, 2015. Continental-scale temperature variability in
1321 PMIP3 simulations and PAGES 2k regional temperature reconstructions over
1322 the past millennium. *Climate of the Past* 11, 1673–1699. doi:10.5194/
1323 **cp**-11-1673-2015.

1324 PAGES2k, 2013. Continental-scale temperature variability during the past two
1325 millennia. *Nature Geoscience* 6, 339–346.

1326 Pausata, F.S.R., Chafik, L., Caballero, R., Battisti, D.S., 2015. Impacts of high-
1327 latitude volcanic eruptions on ENSO and AMOC. *Proceedings of the National*
1328 *Academy of Sciences* 112, 13784–13788. doi:10.1073/**pnas**.1509153112.

1329 Payette, S., 2007. Contrasted dynamics of northern Labrador tree lines caused
1330 by climate change and migrational lag. *Ecology* 88, 770–780.

1331 Pederson, N., Hessel, A.E., Baatarbileg, N., Anchukaitis, K.J., Cosmo, N.D.,
1332 2014. Pluvials, droughts, the Mongol Empire, and modern Mongolia. *Pro-*
1333 *ceedings of the National Academy of Sciences* 111, 4375–4379. doi:10.1073/
1334 **pnas**.1318677111.

1335 Phipps, S.J., McGregor, H.V., Gergis, J., Gallant, A.J., Neukom, R., Steven-
1336 son, S., Ackerley, D., Brown, J.R., Fischer, M.J., Van Ommen, T.D., 2013.

1337 Paleoclimate data–model comparison and the role of climate forcings over the
1338 past 1500 years. *Journal of Climate* 26, 6915–6936.

1339 Plummer, C.T., Curran, M.A.J., van Ommen, T.D., Rasmussen, S.O., Moy,
1340 A.D., Vance, T.R., Clausen, H.B., Vinther, B.M., Mayewski, P.A., 2012. An
1341 independently dated 2000-yr volcanic record from Law Dome, East Antarc-
1342 tica, including a new perspective on the dating of the 1450s CE eruption
1343 of Kuwae, Vanuatu. *Climate of the Past* 8, 1929–1940. doi:10.5194/
1344 cp-8-1929-2012.

1345 Pongratz, J., Reick, C., Raddatz, T., Claussen, M., 2008. A reconstruction
1346 of global agricultural areas and land cover for the last millennium. *Global*
1347 *Biogeochem. Cycles* 22. doi:10.1029/2007gb003153.

1348 Raspopov, O., Dergachev, V., Esper, J., Kozyreva, O., Frank, D., Ogurtsov,
1349 M., Kolström, T., Shao, X., 2008. The influence of the de Vries (~ 200 -year)
1350 solar cycle on climate variations: Results from the Central Asian Mountains
1351 and their global link. *Palaeogeography, Palaeoclimatology, Palaeoecology* 259,
1352 6–16.

1353 Rimbu, N., Lohmann, G., Felis, T., Pätzold, J., 2003. Shift in ENSO tele-
1354 connections recorded by a northern Red Sea coral. *Journal of Climate* 16,
1355 1414–1422. doi:10.1175/1520-0442(2003)16<1414:sietrb>2.0.co;2.

1356 Rind, D., Lean, J., Healy, R., 1999. Simulated time-dependent climate response
1357 to solar radiative forcing since 1600. *Geophys. Res. Lett.* 104, 1973–1990.

1358 Rind, D., Shindell, D., Perlwitz, J., Lerner, J., Lonergan, P., Lean, J., McLin-
1359 den, C., 2004. The relative importance of solar and anthropogenic forcing of
1360 climate change between the Maunder Minimum and the present. *J. Climate*
1361 17, 906–929.

1362 Robock, A., 2000. Volcanic eruptions and climate. *Rev. Geophys* 38, 191–219.

1363 Rutherford, S., Mann, M.E., Delworth, T.L., Stouffer, R.J., 2003. Climate field
1364 reconstruction under stationary and nonstationary forcing. *J. Climate* 16,
1365 462–479.

1366 Rydval, M., Larsson, L.Å., McGlynn, L., Gunnarson, B.E., Loader, N.J., Young,
1367 G.H., Wilson, R., 2014. Blue intensity for dendroclimatology: Should we
1368 have the blues? Experiments from Scotland. *Dendrochronologia* 32, 191–204.
1369 doi:10.1016/j.dendro.2014.04.003.

1370 Schmidt, G.A., 2010. Enhancing the relevance of palaeoclimate model/data
1371 comparisons for assessments of future climate change. *J. Quaternary Sci.* 25,
1372 79–87.

1373 Schmidt, G.A., Annan, J.D., Bartlein, P.J., Cook, B.I., Guilyardi, E., Harg-
1374 reaves, J.C., Harrison, S.P., Kageyama, M., LeGrande, A.N., Konecky, B.,
1375 Lovejoy, S., Mann, M.E., Masson-Delmotte, V., Risi, C., Thompson, D.,
1376 Timmermann, A., Tremblay, L.B., Yiou, P., 2014. Using palaeo-climate com-
1377 parisons to constrain future projections in CMIP5. *Climate of the Past* 10,
1378 221–250. doi:10.5194/cp-10-221-2014.

1379 Schmidt, G.A., Jungclaus, J.H., Ammann, C.M., Bard, E., Braconnot, P.,
1380 Crowley, T.J., Delaygue, G., Joos, F., Krivova, N.A., Muscheler, R., Otto-
1381 Bliesner, B.L., Pongratz, J., Shindell, D.T., Solanki, S.K., Steinhilber, F.,
1382 Vieira, L.E.A., 2012. Climate forcing reconstructions for use in PMIP sim-
1383 ulations of the Last Millennium (v1.1). *Geoscientific Model Development* 5,
1384 185–191.

1385 Schneider, D.P., Ammann, C.M., Otto-Bliesner, B.L., Kaufman, D.S., 2009.
1386 Climate response to large, high-latitude and low-latitude volcanic eruptions
1387 in the Community Climate System Model. *J. Geophys. Res.* 114. doi:10.
1388 1029/2008JD011222.

1389 Schneider, L., Smerdon, J.E., Büntgen, U., Wilson, R.J.S., Myglan, V.S.,
1390 Kirdyanov, A.V., Esper, J., 2015. Revising midlatitude summer tempera-

1391 tures back to A.D. 600 based on a wood density network. *Geophys. Res. Lett.*
1392 42, 4556–4562. doi:10.1002/2015gl063956.

1393 Schneider, T., 2001. Analysis of incomplete climate data: Estimation of mean
1394 values and covariance matrices and imputation of missing values. *J. Climate*
1395 14, 853–871.

1396 Schurer, A.P., Hegerl, G.C., Mann, M.E., Tett, S.F., Phipps, S.J., 2013. Separat-
1397 ing forced from chaotic climate variability over the past millennium. *Journal*
1398 *of Climate* 26, 6954–6973.

1399 Schurer, A.P., Tett, S.F.B., Hegerl, G.C., 2014. Small influence of solar vari-
1400 ability on climate over the past millennium. *Nature Geoscience* 7, 104–108.
1401 doi:10.1038/ngeo2040.

1402 Schweingruber, F., Briffa, K., Nogler, P., 1993. A tree-ring densitometric tran-
1403 sect from Alaska to Labrador. *International Journal of Biometeorology* 37,
1404 151–169.

1405 Schweingruber, F., Fritts, H., Bräker, O., Drew, L., Schär, E., 1978. The X-ray
1406 technique as applied to dendroclimatology. *Tree-Ring Bulletin* 38, 61–91.

1407 Seager, R., Burgman, R., Kushnir, Y., Clement, A., Cook, E., Naik, N., Miller,
1408 J., 2008. Tropical Pacific forcing of North American medieval megadroughts:
1409 Testing the concept with an atmosphere model forced by coral-reconstructed
1410 SSTs. *J. Climate* 21, 6175–6190.

1411 Seager, R., Graham, N., Herweijer, C., Gordon, A.L., Kushnir, Y., Cook, E.R.,
1412 2007. Blueprints for Medieval hydroclimate. *Quat. Sci. Rev.* 26, 2322–2336.

1413 Shindell, D., Faluvegi, G., 2009. Climate response to regional radiative forcing
1414 during the twentieth century. *Nature Geoscience* 2, 294–300.

1415 Shindell, D.T., 2014. Inhomogeneous forcing and transient climate sensitivity.
1416 *Nature Climate Change* 4, 274–277.

1417 Shindell, D.T., Faluvegi, G., Rotstayn, L., Milly, G., 2015. Spatial patterns of
1418 radiative forcing and surface temperature response. *Journal of Geophysical*
1419 *Research: Atmospheres* 120, 5385–5403.

1420 Shindell, D.T., Schmidt, G.A., Mann, M.E., Faluvegi, G., 2004. Dynamic winter
1421 climate response to large tropical volcanic eruptions since 1600. *J. Geophys.*
1422 *Res. - Atmospheres* 109. doi:10.1029/2003JD004151.

1423 Shindell, D.T., Schmidt, G.A., Mann, M.E., Rind, D., Waple, A., 2001a. Solar
1424 forcing of regional climate change during the Maunder Minimum. *Science*
1425 294, 2149–2152.

1426 Shindell, D.T., Schmidt, G.A., Miller, R.L., Mann, M.E., 2003. Volcanic and
1427 solar forcing of climate change during the preindustrial era. *J. Climate* 16,
1428 4094–4107.

1429 Shindell, D.T., Schmidt, G.A., Miller, R.L., Rind, D., 2001b. Northern Hemi-
1430 sphere winter climate response to greenhouse gas, ozone, solar, and volcanic
1431 forcing. *J. Geophys. Res. - Atmospheres* 106, 7193–7210.

1432 Sigl, M., Winstrup, M., McConnell, J.R., Welten, K.C., Plunkett, G., Lud-
1433 low, F., Büntgen, U., Caffee, M., Chellman, N., Dahl-Jensen, D., Fischer,
1434 H., Kipfstuhl, S., Kostick, C., Maselli, O.J., Mekhaldi, F., Mulvaney, R.,
1435 Muscheler, R., Pasteris, D.R., Pilcher, J.R., Salzer, M., Schüpbach, S., Stef-
1436 fensen, J.P., Vinther, B.M., Woodruff, T.E., 2015. Timing and climate forc-
1437 ing of volcanic eruptions for the past 2,500 years. *Nature* 523, 543–549.
1438 doi:10.1038/nature14565.

1439 Smerdon, J.E., Kaplan, A., Amrhein, D.E., 2010. Erroneous model field repre-
1440 sentations in multiple pseudoproxy studies: Corrections and implications. *J.*
1441 *Climate* 23, 5548–5554. doi:10.1175/2010JCLI3742.1.

1442 Smerdon, J.E., Kaplan, A., Chang, D., 2008. On the origin of the standard-
1443 ization sensitivity in RegEM climate field reconstructions. *J. Climate* 21,
1444 6710–6723.

1445 Smerdon, J.E., Kaplan, A., Zorita, E., González-Rouco, J.F., Evans, M.N., 2011.
1446 Spatial performance of four climate field reconstruction methods targeting the
1447 Common Era. *Geophys. Res. Lett.* 38. doi:10.1029/2011GL047372.

1448 Smerdon, J.E., Pollack, H.N., 2016. Reconstructing Earth’s surface temperature
1449 over the past 2000 years: the science behind the headlines. *Wiley Interdisci-*
1450 *plinary Reviews: Climate Change* doi:10.1002/wcc.418.

1451 Solomon, A., Goddard, L., Kumar, A., Carton, J., Deser, C., Fukumori, I.,
1452 Greene, A., Hegerl, G., Kirtman, B., Kushnir, Y.M.N., Smith, D., Vimont,
1453 D., Delworth, T., Meehl, G.A., Stockdale, T., 2011. Distinguishing the roles
1454 of natural and anthropogenically forced decadal climate variability. *Bulletin*
1455 *of the American Meteorological Society* 92, 141–156.

1456 St. George, S., 2014. An overview of tree-ring width records across the North-
1457 ern Hemisphere. *Quaternary Science Reviews* 95, 132–150. doi:10.1016/j.
1458 *quascirev*.2014.04.029.

1459 St George, S., Ault, T.R., 2014. The imprint of climate within Northern Hemi-
1460 sphere trees. *Quaternary Science Reviews* 89, 1–4.

1461 St. George, S., Ault, T.R., Torbenson, M.C.A., 2013. The rarity of absent
1462 growth rings in Northern Hemisphere forests outside the American Southwest.
1463 *Geophys. Res. Lett.* 40, 3727–3731. doi:10.1002/grl.50743.

1464 Steiger, N.J., Hakim, G.J., Steig, E.J., Battisti, D.S., Roe, G.H., 2014. Assim-
1465 ilation of time-averaged pseudoproxies for climate reconstruction. *Journal of*
1466 *Climate* 27, 426–441. doi:10.1175/jcli-d-12-00693.1.

1467 Steinhilber, F., Beer, J., Fröhlich, C., 2009. Total solar irradiance during the
1468 Holocene. *Geophys. Res. Lett.* 36. doi:10.1029/2009gl040142.

1469 Stenchikov, G., Hamilton, K., Stouffer, R.J., Robock, A., Ramaswamy, V.,
1470 Santer, B., Graf, H.F., 2006. Arctic Oscillation response to volcanic eruptions
1471 in the IPCC AR4 climate models. *J. Geophys. Res.* 111, D07107. doi:10.
1472 1029/2005JD006286.

- 1473 Stoffel, M., Khodri, M., Corona, C., Guillet, S., Poulain, V., Bekki, S., Guiot,
1474 J., Luckman, B.H., Oppenheimer, C., Lebas, N., Beniston, M., Masson-
1475 Delmotte, V., 2015. Estimates of volcanic-induced cooling in the North-
1476 ern Hemisphere over the past 1,500 years. *Nature Geoscience* 8, 784–788.
1477 doi:10.1038/ngeo2526.
- 1478 von Storch, H., Zorita, E., Jones, J.M., Dimitriev, Y., Gonzalez-Rouco, F.,
1479 Tett, S.F.B., 2004. Reconstructing past climate from noisy data. *Science* 306,
1480 679–682.
- 1481 Stott, P.A., Gillett, N.P., Hegerl, G.C., Karoly, D.J., Stone, D.A., Zhang, X.,
1482 Zwiers, F., 2010. Detection and attribution of climate change: a regional
1483 perspective. *Wiley Interdisciplinary Reviews: Climate Change* 1, 192–211.
- 1484 Stott, P.A., Jones, G.S., 2009. Variability of high latitude amplification of
1485 anthropogenic warming. *Geophys. Res. Lett.* 36. doi:10.1029/2009g1037698.
- 1486 Stott, P.A., Tett, S.F.B., 1998. Scale-dependent detection of climate change.
1487 *Journal of Climate* 11, 3282–3294. doi:10.1175/1520-0442(1998)011<3282:
1488 sddocc>2.0.co;2.
- 1489 Stuiver, M., Braziunas, T.F., 1993. Sun, ocean, climate and atmospheric $^{14}\text{CO}_2$:
1490 an evaluation of causal and spectral relationships. *The Holocene* 3, 289–305.
- 1491 Sundqvist, H.S., Kaufman, D.S., McKay, N.P., Balascio, N.L., Briner, J.P.,
1492 Cwynar, L.C., Sejrup, H.P., Seppä, H., Subetto, D.A., Andrews, J.T., Ax-
1493 ford, Y., Bakke, J., Birks, H.J.B., Brooks, S.J., de Vernal, A., Jennings,
1494 A.E., Ljungqvist, F.C., Rühland, K.M., Saenger, C., Smol, J.P., Viau, A.E.,
1495 2014. Arctic Holocene proxy climate database: new approaches to assess-
1496 ing geochronological accuracy and encoding climate variables. *Climate of the*
1497 *Past* 10, 1605–1631. doi:10.5194/cp-10-1605-2014.
- 1498 Swingedouw, D., Terray, L., Cassou, C., Voldoire, A., Salas-Mélia, D., Ser-
1499 vonnat, J., 2010. Natural forcing of climate during the last millennium:

1500 fingerprint of solar variability. *Clim Dyn* 36, 1349–1364. doi:10.1007/
1501 s00382-010-0803-5.

1502 Szeicz, J.M., MacDonald, G.M., 1995. Recent white spruce dynamics at the
1503 subarctic alpine treeline of north-western Canada. *Journal of Ecology* 83,
1504 873–885. doi:10.2307/2261424.

1505 Tierney, J.E., Abram, N.J., Anchukaitis, K.J., Evans, M.N., Giry, C., Kilbourne,
1506 K.H., Saenger, C.P., Wu, H.C., Zinke, J., 2015. Tropical sea surface temper-
1507 atures for the past four centuries reconstructed from coral archives. *Paleo-*
1508 *ceanography* 30, 226–252. doi:10.1002/2014pa002717.

1509 Tingley, M., Craigmile, P.F., Haran, M., Li, B., Mannshardt, E., Rajaratnam,
1510 B., 2015. On Discriminating between GCM Forcing Configurations Using
1511 Bayesian Reconstructions of Late-Holocene Temperatures. *Journal of Climate*
1512 28, 8264–8281. doi:10.1175/jcli-d-15-0208.1.

1513 Tingley, M.P., Craigmile, P.F., Haran, M., Li, B., Mannshardt, E., Rajaratnam,
1514 B., 2012. Piecing together the past: Statistical insights into paleoclimatic
1515 reconstructions. *Quat. Sci. Rev.* 35, 1–22.

1516 Tingley, M.P., Huybers, P., 2010. A Bayesian Algorithm for Reconstructing
1517 Climate Anomalies in Space and Time. Part I: Development and Applications
1518 to Paleoclimate Reconstruction Problems. *J. Climate* 23, 2759–2781. doi:10.
1519 1175/2009JCLI3015.1.

1520 Tingley, M.P., Huybers, P., 2013. Recent temperature extremes at high northern
1521 latitudes unprecedented in the past 600 years. *Nature* 496, 201–205. doi:10.
1522 1038/nature11969.

1523 Torrence, C., Compo, G., 1998. A practical guide to wavelets. *Bull. Amer.*
1524 *Meteorol. Soc.* 79, 61–78.

1525 Touchan, R., Anchukaitis, K.J., Shishov, V.V., Sivrikaya, F., Attieh, J., Ket-
1526 men, M., Stephan, J., Mitsopoulos, I., Christou, A., Meko, D.M., 2014. Spa-

1527 tial Patterns of eastern Mediterranean climate influence on tree growth. The
1528 Holocene 24, 381–392. doi:10.1177/0959683613518594.

1529 Trenberth, K.E., 1984. Some Effects of Finite Sample Size and Persistence
1530 on Meteorological Statistics. Part I: Autocorrelations. Mon. Wea. Rev. 112,
1531 2359–2368. doi:10.1175/1520-0493(1984)112<2359:seofss>2.0.co;2.

1532 Verosub, K.L., Lippman, J., 2008. Global impacts of the 1600 eruption of Peru’s
1533 Huaynaputina volcano. Eos, Transactions American Geophysical Union 89,
1534 141–142.

1535 Vieira, L.E.A., Solanki, S.K., 2010. Evolution of the solar magnetic flux on
1536 time scales of years to millenia. Astronomy and Astrophysics 509, A100.
1537 doi:10.1051/0004-6361/200913276.

1538 Wagner, G., Beer, J., Masarik, J., Muscheler, R., Kubik, P.W., Mende, W., Laj,
1539 C., Raisbeck, G.M., Yiou, F., 2001. Presence of the solar de vries cycle (~205
1540 years) during the last ice age. Geophys. Res. Lett. 28, 303–306. doi:10.1029/
1541 2000gl1006116.

1542 Wagner, S., Zorita, E., 2005. The influence of volcanic, solar and CO2 forcing
1543 on the temperatures in the Dalton Minimum (1790–1830): a model study.
1544 Climate Dyn. 25, 205–218.

1545 Wang, J., Emile-Geay, J., Guillot, D., McKay, N.P., Rajaratnam, B., 2015.
1546 Fragility of reconstructed temperature patterns over the Common Era: Im-
1547 plications for model evaluation. Geophysical Research Letters 42, 7162–7170.

1548 Waple, A., Mann, M.E., Bradley, R.S., 2002. Long-term Patterns of Solar Irra-
1549 diance Forcing in Model Experiments and Proxy-based Surface Temperature
1550 Reconstructions. Clim. Dynam. 18, 563–578.

1551 Wiles, G.C., D’Arrigo, R.D., Barclay, D., Wilson, R.S., Jarvis, S.K., Vargo,
1552 L., Frank, D., 2014. Surface air temperature variability reconstructed with
1553 tree rings for the Gulf of Alaska over the past 1200 years. The Holocene 24,
1554 198–208. doi:10.1177/0959683613516815.

1555 Wilson, R., Anchukaitis, K., Briffa, K.R., Büntgen, U., Cook, E., D'Arrigo,
 1556 R., Davi, N., Esper, J., Frank, D., Gunnarson, B., Hegerl, G., Helama, S.,
 1557 Klesse, S., Krusic, P.J., Linderholm, H.W., Myglan, V., Osborn, T.J., Rydval,
 1558 M., Schneider, L., Schurer, A., Wiles, G., Zhang, P., Zorita, E., 2016. Last
 1559 millennium northern hemisphere summer temperatures from tree rings: Part
 1560 I: The long term context. *Quaternary Science Reviews* 134, 1–18. doi:10.
 1561 1016/j.quascirev.2015.12.005.

1562 Wilson, R., Cook, E., D'Arrigo, R., Riedwyl, N., Evans, M.N., Tudhope, A.,
 1563 Allan, R., 2010. Reconstructing ENSO: the influence of method, proxy data,
 1564 climate forcing and teleconnections. *J. Quaternary Sci.* 25, 62–78. doi:10.
 1565 1002/jqs.1297.

1566 Wilson, R., D'Arrigo, R.D., Buckley, B.M., Büntgen, U., Esper, J., Frank,
 1567 D., Luckman, B., Payette, S., Vose, R., Youngblut, D., 2007. A matter of
 1568 divergence: Tracking recent warming at hemispheric scales using tree ring
 1569 data. *Journal of Geophysical Research* 112. doi:10.1029/2006JD008318.

1570 Wilson, R., Rao, R., Rydval, M., Wood, C., Larsson, L.A., Luckman, B.H.,
 1571 2014. Blue Intensity for dendroclimatology: The BC blues: A case study
 1572 from British Columbia, Canada. *The Holocene* 24, 1428–1438. doi:10.1177/
 1573 0959683614544051.

1574 Wilson, R., Tudhope, A., Brohan, P., Briffa, K.R., Osborn, T.J., Tett, S., 2006.
 1575 Two-hundred-fifty years of reconstructed and modeled tropical temperatures.
 1576 *J. Geophys. Res.* 111, C10007. doi:10.1029/2005JC003188.

1577 Wise, E.K., 2015. Tropical Pacific and Northern Hemisphere influences on the
 1578 coherence of Pacific Decadal Oscillation reconstructions. *International Jour-
 1579 nal of Climatology* 35, 154–160.

1580 Youngblut, D., Luckman, B., 2008. Maximum June-July temperatures in the
 1581 southwest Yukon over the last 300 years reconstructed from tree rings. *Den-
 1582 drochronologia* 25, 153–166. doi:10.1016/j.dendro.2006.11.004.

- 1583 Zanchettin, D., Timmreck, C., Graf, H.F., Rubino, A., Lorenz, S., Lohmann,
1584 K., Krüger, K., Jungclaus, J.H., 2012. Bi-decadal variability excited in the
1585 coupled ocean–atmosphere system by strong tropical volcanic eruptions. *Clim*
1586 *Dyn* 39, 419–444. doi:10.1007/s00382-011-1167-1.
- 1587 Zhang, P., Linderholm, H.W., Gunnarson, B.E., Björklund, J., Chen, D.,
1588 2016. 1200 years of warm-season temperature variability in central Scan-
1589 dinavia inferred from tree-ring density. *Climate of the Past* 12, 1297–1312.
1590 doi:10.5194/cp-12-1297-2016.
- 1591 Zorita, E., González-Rouco, F., Legutke, S., 2003. Testing the Mann et al.
1592 [1998] approach to paleoclimate reconstructions in the context of a 1000-yr
1593 control simulation with the ECHO-G Coupled Climate Model. *J. Climate* 16,
1594 1378–1390.
- 1595 Zwiers, F.W., Weaver, A.J., 2000. The causes of 20th century warming. *Science*
1596 290, 2081–2083.